DETERMINING PEN SURFACE WATER IN A CATTLE FEEDLOT WITH THERMAL INFRARED REMOTE SENSING

by

CURTIS JOSEPH LEIKER

B.S., Kansas State University, 2008

A THESIS

submitted in partial fulfillment of the requirements for the degree

MASTER OF SCIENCE

Department of Biological and Agricultural Engineering
College of Engineering

KANSAS STATE UNIVERSITY
Manhattan, Kansas

2010

Approved by:

Major Professor
Dr. Ronaldo Maghirang

Copyright

Abstract

Particulate matter (PM) emissions from open beef cattle feedlots depend heavily on the level of water on the pen surface. Wet pen surfaces are able to keep PM emissions low, while dry surfaces have much higher rates of emission. Current research shows that 20-25% surface water content is a critical threshold for minimizing PM emissions from open cattle feedlots. The amount of water on the pen surface will also dictate the level of gaseous emissions, such as ammonia, nitrous oxide, and hydrogen sulfide. Traditional methods of measuring pen surface water are not sufficient within a dense cattle feedlot and cannot provide a continuous method of measurement unattended. The process of using infrared thermometry and meteorological variables to remotely sense surface water provides an inexpensive, ground level approach.

Testing in laboratory, outdoor, and feedlot conditions was conducted to analyze the potential of using the thermal inertia remote sensing approach. This approach involved continuous measurement of weighted soil water content, surface temperature of the soil, air temperature, solar radiation, wind speed, and relative humidity. Controlled laboratory testing performed the best at predicting soil water content from the difference in soil surface and air temperature, with the coefficient of determination (R^2) at 0.91 for a Smolan silt loam and 0.83 for dry feedlot soil. Outdoor testing achieved mixed results with R^2 values only as high as 0.38 for 10-cm soil layer and 0.67 for 5-cm soil layer. Testing in a cattle feedlot with dry, loose manure layer proved to be imprecise, but was able to differentiate surface water levels varying from 4.1% to 9.1% wet basis.

Table of Contents

List of Figures

List of Tables

Acknowledgements

A special thanks to my Major Professor Dr. Ronaldo Maghirang for his guidance and support as I pursued my M.S. degree as well as Dr. Danny Rogers and Dr. Kevin Price for taking time to serve on my graduate committee. Thanks to Edna, Li, Henry, Orlando, and Howell for making the trips to the feedlots fun and enjoyable. I would like to acknowledge Darrell Oard for all his help in the laboratory. To Mary Knapp of Agronomy for allowing me to use the department's soil water probe as well as helping with data collection from the weather station. To David for constructing my outdoor metal frame. To everyone in the KSU Air Team for their ideas and help. Finally to the USDA's National Institute of Food and Agriculture (NIFA) for providing funding for this research.

CHAPTER 1 - Introduction

1.1 Background

As both the United States and the world's populations continue to grow, increasing the world's food supply is a top priority for agriculture. Open-lot animal feeding operations (AFOs) play an important role in providing large sources of food.

1.1.1 Animal Feeding Operations

AFOs are driven by economic factors in open markets for meats, poultry, milk, and eggs. They are more efficient and cost effective than traditional methods for raising animals. As urban areas expand, many people are living closer to these operations and exposed to air quality and other environmental issues. The Environmental Protection Agency (EPA) defines AFOs as 1) animals are kept 45 days of the year or more and 2) structures or animal traffic prevents vegetative growth (NRC, 2003).

From 1982 to 1997, livestock production from AFOs slightly increased by 10%, while the actual number of AFOs decreased by half. As of 2003, there are approximately 450,000 AFOs in the U.S. Livestock agriculture and resulting products from agriculture accounted for over $90 billion into the U.S. economy annually in the late 1990's and is a major consumer of the U.S. crop agriculture. According to the U.S. Department of Agriculture (USDA) in 2001, U.S. per capita consumption of beef was 30.0 kg. Beef cattle reached a zenith in 1975 when there were 132 million cattle within the U.S, while in 2001 the number had been reduced to 96.7 million. Operations with more than 50 head account for 88.5% of all cattle (NRC, 2003). Figures 1.1, 1.2, and 1.3 show USDA cattle inventory statistics for the last 20 years from 1990 to 2010. Total cattle inventory has slightly decreased to approximately 101 million in 2009 while the total number of cattle operations has dropped from over 1.3 million in 1989 to 950,000 in 2009.

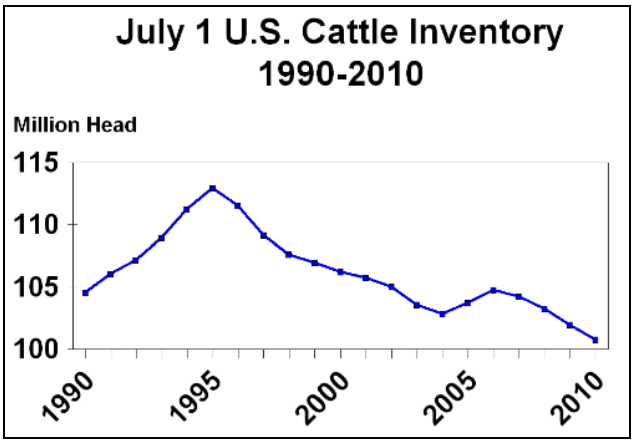

Figure 1.1 U.S. Cattle Inventory as of July 1.

(Source: http://www.usda.gov)

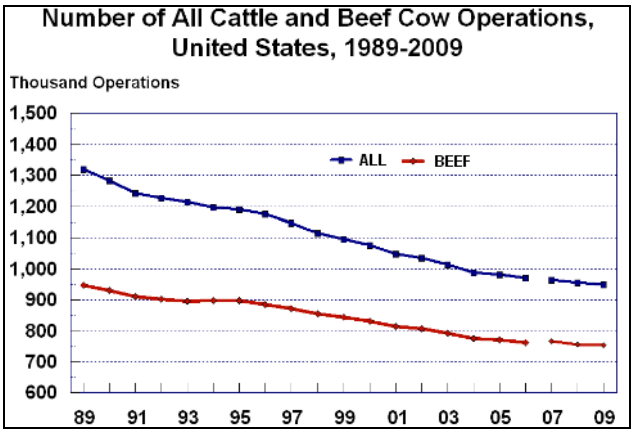

Figure 1.2 Total Number of Cattle and Beef Cow Operations.

(Source: http://www.usda.gov)

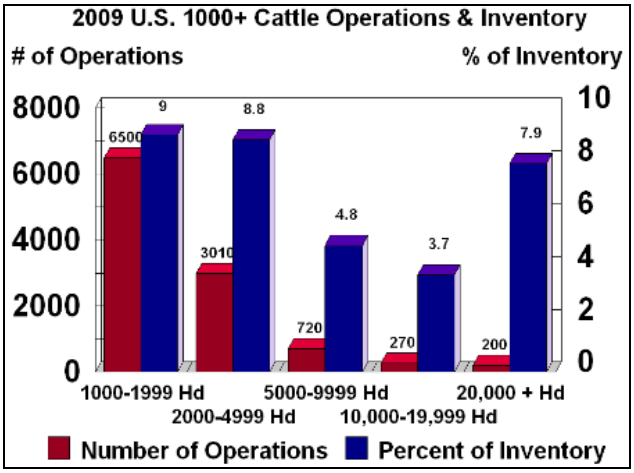

Figure 1.3 U.S. 1000+ Cattle Operations and Inventory.

(Source: http://www.usda.gov)

1.1.2 Environmental Problems

The EPA officially announced an air quality compliance agreement on January 21, 2005 on certain AFOs, including swine, poultry, and dairy cattle. The following were the main goals sought from the agreement:

- Reduce air pollution
- Ensure compliance with applicable provisions in the Clean Air Act, Comprehensive Environmental Response, Compensation and Liability Act (CERCLA), and Environmental Planning and Community Right-to-Know Act (EPCRA)
- Monitor and evaluate AFO emissions
- Promote a national consensus on methodologies for estimating emissions from AFOs (EPA, 2009)

Under the agreement, scientists have monitored air emissions in several facilities for dairy, swine, and poultry. In order to effectively manage AFOs, one must know the factors that may influence emissions from the AFO. Geographic and climatic characteristics can vary from region to region within the U.S. Whether the operation is in the hot and dry panhandle of Texas or the cool and wet regions of the northern Midwest will impact how and when air pollutants are emitted. Temperature, wind velocity, soil type, rainfall intensity and frequency, and topography all play an important role. If a region is hot and wet, emissions of gaseous air pollutants will increase accordingly. Evapotranspiration rates or the availability of having large areas for land application for the manure can change management practices and emission rates. Besides long term fluctuations in climate, AFOs experience many short term changes that influence emission rates of air pollutants. Seasonal and daily temperature swings, daily weather patterns, and daily cycles of the animals' eating and behavior patterns all influence emissions. Having animals at different stages in their maturation results in different amounts of fecal matter and urine excreted. With animals at different stages of growth, moving them in and out of the confinement units causes variations. An AFO may only be at full capacity at certain times of the year depending on the markets and management (NRC, 2003).

Although AFOs have been subject to regulation under the Clean Water Act for several years, no such regulations on air quality are enforced. Rural residents living near AFOs have become less tolerant over the years of odors and dust emitted due to health reasons, quality of

life, or decreased property values. The list of air pollutants generated from AFOs include ammonia, hydrogen sulfide, particulate matter (PM), volatile organic compounds (VOC), and greenhouse gases (carbon dioxide, nitrous oxide, methane) (Cole et al., 2008).

"Criteria" pollutants, such as PM_{10} and $PM_{2.5}$ (PM with equivalent aerodynamic diameter of 10 and 2.5 μm, respectively, or less), ozone, carbon monoxide, nitrogen dioxide, sulfur dioxide, and lead are regulated under the authority of the Clear Air Act of 1970. Primary and secondary air quality standards have been set by the EPA under the National Ambient Air Quality Standards (NAAQS). Primary standards set limits to protect public health, including health of "sensitive" populations such as asthmatics, children, and the elderly. Secondary standards set limits to protect public welfare, including protection against decreased visibility, damage to animals, crops, vegetation, and buildings (EPA, 2010). Historically, agriculture has been exempted from this regulation. As of the late 1990's, the EPA did not have sufficient data to create reasonable regulatory requirements for AFOs. In 2004, the EPA ruled in favor of including agricultural sources to the NAAQS regulation of PM_{10} (Cole et al., 2008). Current standards for PM_{10} are set at 150 $\mu g/m^3$ as a 24-h average for both primary and secondary standards. $PM_{2.5}$ is set at 35 $\mu g/m^3$ as a 24-h average for primary and secondary standards as well as 15.0 $\mu g/m^3$ as an annual average for primary and secondary standards (EPA, 2010).

Since urban areas have the highest population density there tends to be more ambient monitoring stations located in those areas; however, the correct meaning of "ambient" is any area in which the public can access. This means that air quality near a property line of an air polluting source in a scarce population area is subject to the same regulation as in an urban center. The state air pollution regulatory authorities (SAPRAs) are the agencies that do most of the law enforcement. The states are allowed to set their own air quality standards as long as they are at least as stringent as the federal standards. The states set up ambient monitoring programs, operation permits, and complete inspections for compliance (Auvermann, 2001).

1.1.3 Surface Water and Environmental Problems

There are numerous parameters that influence the PM emission rate from a beef cattle feedlot, with pen surface water content being one of the most important. With low surface water conditions, dust emissions dominate air quality problems. With high surface water, odor and gaseous emissions dominate. Since odor compounds attach to dust particles, odor will never be

totally eliminated. The ideal water range to minimize air quality problems is between 25% and 40% on a wet basis, as shown in Figure 1.4 (Auvermann, 2001).

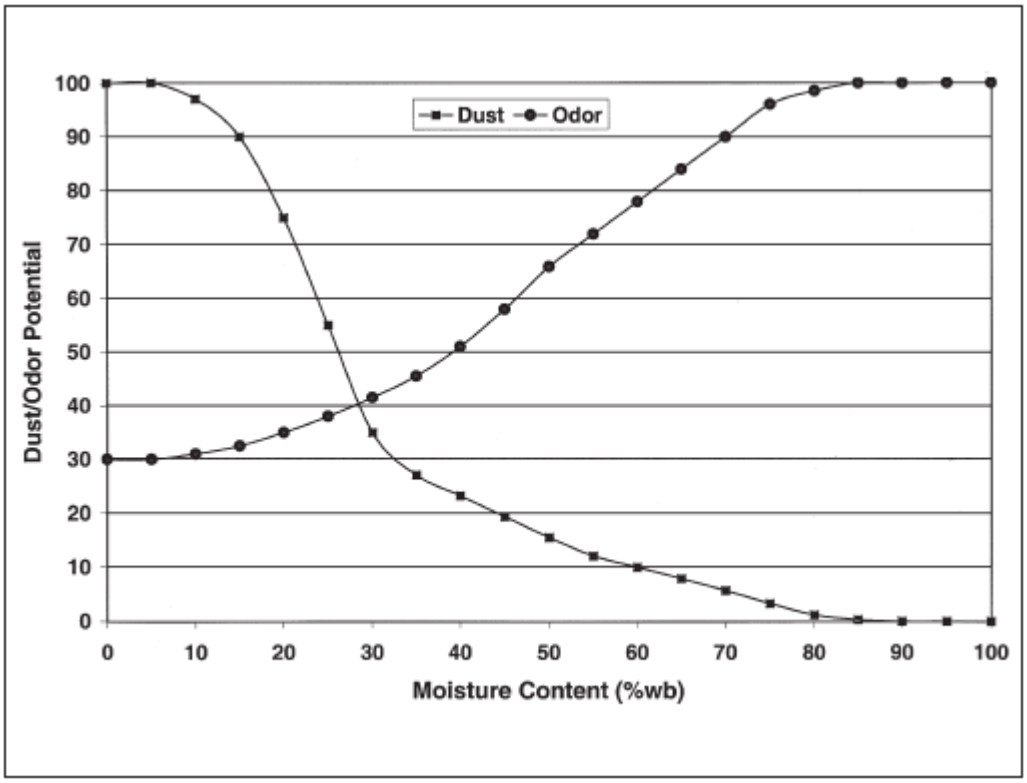

Figure 1.4 Conceptual, qualitative relationship between dust potential and odor potential as a function of the water content of an open lot corral surface.

(Source: Auvermann, 2001)

Water is one of many dust suppressants that could be used on a feedlot pen surface. It agglomerates surface particles, thereby minimizing emission rates. Applying water to the pen surface however, can only control dust for a relatively short time due to evaporation that depends on many meteorological factors. Bolander and Yamada (1999) indicated that regular, light watering is more effective than intermittent, heavy watering for unpaved roads. Bonifacio (2009) showed that both rainfall and water application can significantly reduce downwind PM_{10} concentrations of commercial cattle feedlots in Kansas. For water application, PM_{10} was reduced by 32% to 80% with a maximum rate of 5 mm/day applied at 1.25 mm every 4 hours, but effects only persisted for one day. For rainfall events, PM_{10} was reduced by 17% to 96% with effects lasting up to seven days.

Knowing the impact of water application onto the pen surface will allow for maximum reduction in air pollutants with minimum usage of water. With many AFOs in dry climates,

preserving water resources becomes critical. But in order to know the pen surface water level, there must be an accurate measurement technique. Traditional contact methods for measuring soil water include oven-drying, soil water tension, radiation, and electrical characterization. Remote sensing methods include near and middle infrared radiometric behavior, thermal inertia, and RADAR. Simulating actual feedlot conditions outside a feedlot is complex due to manure characteristics and compaction from animals (Marek et al., 2004). A feedlot will start to develop a manure/soil interfacial layer over time that will create a water seal near the surface of the pen. A basal layer of medium-sized, compacted particles rests on top of the interfacial layer. This surface layer is easily agitated by cattle hoof movements since it contains powdery and loose materials (Sweeten and Lott, 1994).

1.2 Research Objectives

The main objectives of this research were to (1) develop a cost effective remote sensing technique for measuring pen surface water in a cattle feedlot and to (2) test the technique under laboratory and field conditions.

CHAPTER 2 - Literature Review

2.1 Traditional Contact Methods

Many methods have been established to measure soil water by both weight and volume. These methods include oven-drying, soil water tension, radiation, and electrical characterization of the soil. Research in remote sensing has allowed even more methods to be introduced including near and middle infrared radiometric behavior, thermal inertia, and RADAR.

2.1.1 Gravimetric

The most accurate measure of soil water is the oven-drying method. A wet soil sample is weighed then placed in an oven to be heated at 105°C for 24 hours. The sample is then reweighed to obtain the dry weight. The difference in weight between the wet and dry sample is then taken over the total weight of the soil (either wet or dry weight) to arrive at the water fraction (Ward and Trimble, 2004):

$$\theta g\,(\text{dry basis}) = \frac{m_w}{m_s} \quad \text{OR} \quad \theta g\,(\text{wet basis}) = \frac{m_w}{(m_s + m_w)} \qquad \textbf{(2.1)}$$

where

θ_g = gravimetric soil water content (%)

m_w = mass of water (g)

m_s = mass of dry soil (g)

2.1.2 Gypsum-Porous Blocks

A porous material, that is usually gypsum as shown in Figure 2.1, is placed into the soil along with electrodes that are embedded into the blocks. The blocks will eventually reach the same water level as the surrounding soil. A power source is used on a Wheatstone bridge to measure resistance. Resistance, which is the inverse of conductivity, is related back to the water content in the soil. This technique does not do well detecting small changes in water content, but is best for distinguishing between dry and wet soils (Ward and Trimble, 2004). The method is fast and relatively inexpensive. The blocks do not perform well in coarse or saline soils. They should also be replaced every one to three years (Alshikaili, 2007).

Figure 2.1 Gypsum Blocks

(Source: http://www.ictinternational.com.au)

2.1.3 Neutron Attenuation

Access tubes are placed into the soil with probes that contain an emitter and detector, as shown in Figure 2.2. The radiation source will then emit high energy neutrons that bombard surrounding atoms in the soil. Hydrogen nuclei in the soil are the only substance that will dramatically change the energy level of the neutrons. The percentage of neutrons that see a change in energy will then be recorded by the detector that can be calibrated to the related water content of the soil (Ward and Trimble, 2004). Americium 241, a radioactive source, is used in the process that requires a license and a properly trained user. Since the neutrons do not have an electrical charge, boron tri-fluoride is used to absorb the neutrons that will then cause the gas nucleus to emit photons that can be detected (Alshikaili, 2007).

Figure 2.2 503DR Neutron Probe

(Source: http://www.ictinternational.com.au)

2.1.4 Tensiometers

A porous ceramic cup at the end of a tube filled with water is situated into the soil where a vacuum gauge is applied to the top of the tube. The tensiometer, as shown in Figure 2.3, will then be able to measure the amount of tension that the soil has in order to see how much water is present. They are fairly accurate with wetter soils, but do not do well with dry soils (Alshikaili, 2007).

Figure 2.3 Tensiometer

(Source: http://www.irrometer.com)

2.1.5 Time-Domain Reflectometry

Time-Domain Reflectometry (TDR), as shown in Figure 2.4, uses dual probes placed into the soil while a special apparatus creates a step pulse. The pulse is then returned to the source with a velocity that is unique to the dielectric constant of the soil (Ward and Trimble, 2004).

Figure 2.4 Mini Buriable Waveguide

(Source: http://www.soilmoisture.com)

The dielectric properties of any material can be shown by a complex dielectric or relative permittivity, K* (Ledieu et al., 1986):

$$K^* = K' - j\left(K'' + \left(\frac{\sigma}{\varepsilon_0 \omega}\right)\right) \quad \textbf{(2.2)}$$

where

K' = Real part of relative permittivity

$j = \sqrt{-1}$

K" = Imaginary part of relative permittivity (dielectric loss)

σ = zero frequency conductivity (S/m)

ε_o = permittivity of vacuum (8.85×10^{-12} F/m)

ω = angular frequency (rad/s)

The permittivity shows the polarization of the object that is being subjected to an electric field. There are two main reasons for an electric field creating polarization: (1) electronic, atomic, and molecular distortion of non-polar molecules and (2) rotation of dipolar elements. The dielectric constant of a medium can be defined as (Ledieu et al., 1986):

$$K = \left(\frac{C}{V}\right)^2 \quad \textbf{(2.3)}$$

where

K = Dielectric constant

C = Physical constant (2.998×10^8 m/s)

V = Velocity of electromagnetic waves (m/s)

For soils, there are typically three components that give a soil its overall dielectric constant: air (K = 1), soil particles (K = 3 to 5), and water (K = 81). It is the large differences in the dielectric constant that allows soil water to be plainly detected. Changes in the dielectric constant of water changes with temperature and must be factored into the equations. Adjusting in the range of 0°C to 35°C on the transit time in soil can be done with the following correction factor (Ledieu et al., 1986):

$$tt = \frac{2L}{e}\left[1 + a \cdot \delta + b \cdot \left(1 - \frac{T - T_{ref}}{400}\right) \cdot \theta_v\right] \quad \textbf{(2.4)}$$

where

tt = two-way transit time (ns)

L = probe length (cm)

e = velocity in free space (30 cm/ns)

a = constant based on soil type

δ = bulk density (g/cm^3)

b = coefficient established through calibration

T = temperature of soil (°C)

T_{ref} = reference temperature (soil temperature at calibration, °C)

θ_v = volumetric water content (%)

Using a TDR with two rods and diodes 94% of the electromagnetic wave energy is contained within a diameter equal to twice the distance between the two rods. The bulk density of the soil has a minimal effect on the transit time compared with the water content. An error of 0.1 g/cm^3 in bulk density will only cause a variation of 0.34% in volumetric soil water content (Ledieu et al., 1986).

2.2 Remote Sensing

The term remote sensing is defined by the American Society for Photogrammetry and Remote Sensing (ASPRS) as:

> The measurement or acquisition of information of some property of an object or phenomenon, by a recording device that is not in physical or intimate contact with the object or phenomenon under study (Jensen, 2007).

The term remote sensing first originated in the early 1960's from the unpublished paper by Evelyn L. Pruitt of the Office of Naval Research Geography Branch. This was after a time when aerial photos had been interpreted during World War II, the U.S.S.R had launched *Sputnik* in 1957, and the U.S. launched *Explorer I* in 1958. The Office of Naval Research was increasing its research using several devices that went into different parts of the electromagnetic spectrum

other than visible light. The term photography, that means "to write with [visible] light" became too broad of a term. Thus, the term remote sensing gained momentum and has been the official term coined (Jensen, 2007).

Remote sensing has progressed over time due to many advantages that it can provide. Passive sensors will not disturb the object or area being studied, they simply collect data reflected or emitted. It can also provide enormous amounts of data over large areas at an economical price. It can provide measurements over entire areas, instead of a single point (Jensen, 2007).

Although remote sensing has many advantages, it has limitations. Remote sensing simply allows for spatial, temporal, and spectral information to be collected that must be calibrated, processed, and analyzed by the user. Human error can cause inaccurate data collection once a particular method has been specified by the designers. If an active remote sensing system is needed, it can emit strong electromagnetic radiation that could possibly affect the object or area of interest. Instrumentation can also become uncalibrated over time that will need to be corrected (Jensen, 2007).

When performing a remote sensing technique related to water, it is important to know the light absorption and scattering properties of pure water. As shown in Figure 2.5, molecular water absorption dominates the <400 nm and >580 nm wavelength bands. From approximately 400 to 500 nm wavelengths, level of absorption is minimal. It is these wavelengths from violet to light blue that can penetrate the furthest into a water body. At this range, scattering becomes as important as absorption and is the reason for water's blue color. Nearly all of near and middle infrared (740-2500 nm) is absorbed by water with little scattering (Jensen, 2007).

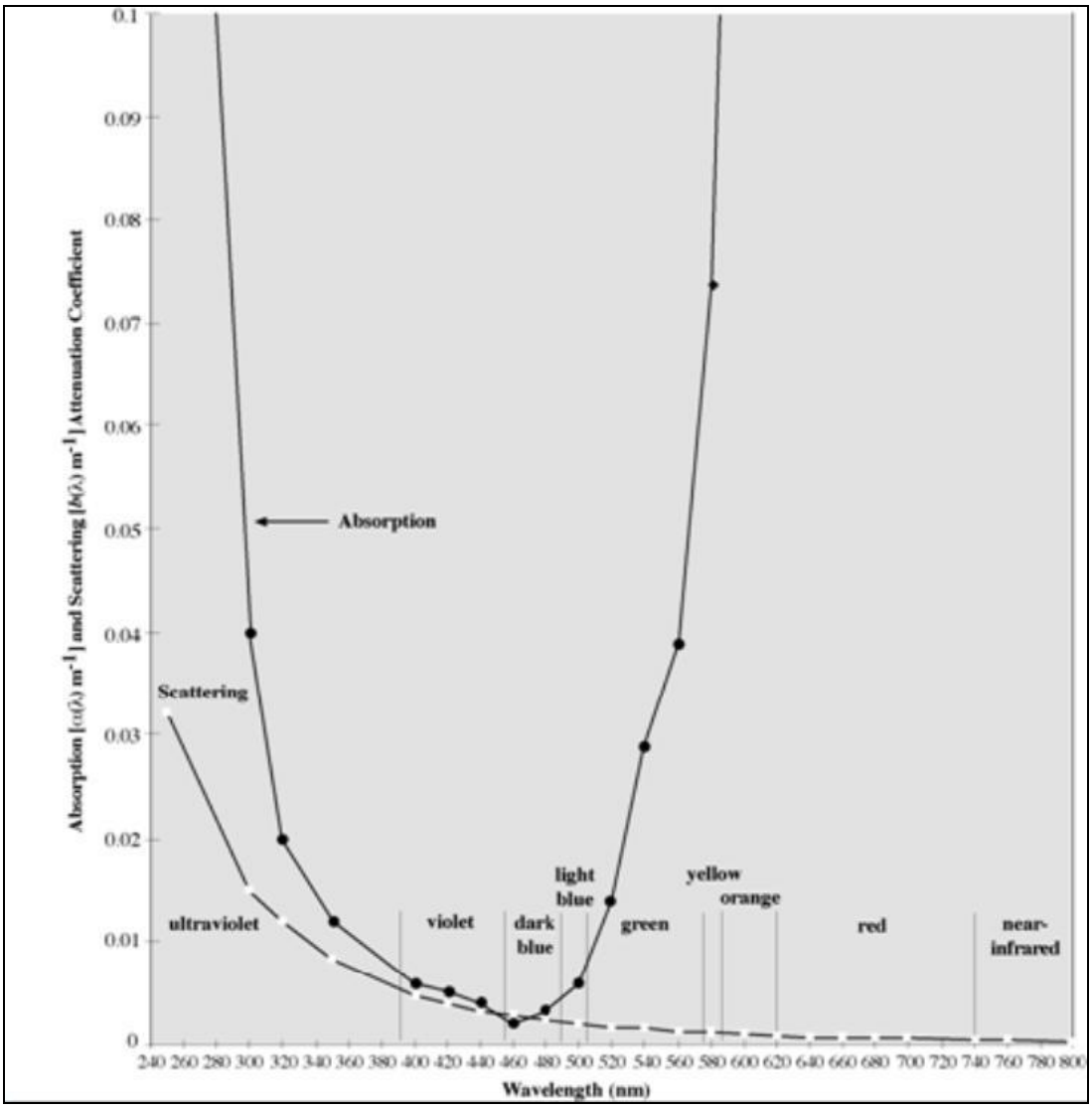

Figure 2.5 Absorption and Scattering of Light in Pure Water

(Source: Jensen, 2007)

2.2.1 Near and Middle Infrared Radiometric Behavior

Bower and Hanks (1965) used a spectrophotometer with a range of 185 to 3500 nm on a Newtonia silt loam to measure the effect of soil water content on reflectance. Figure 2.6 shows where reflectance was measured against varying soil water content. Major water absorption bands were discovered at 1440, 1900, and 2200 nm wavelengths. The 1440 and 1900 nm bands were strongly absorbed and centered around the fundamental frequencies where water molecules vibrate. Results also showed the third absorption band at 2200 nm weakens as soil water increased.

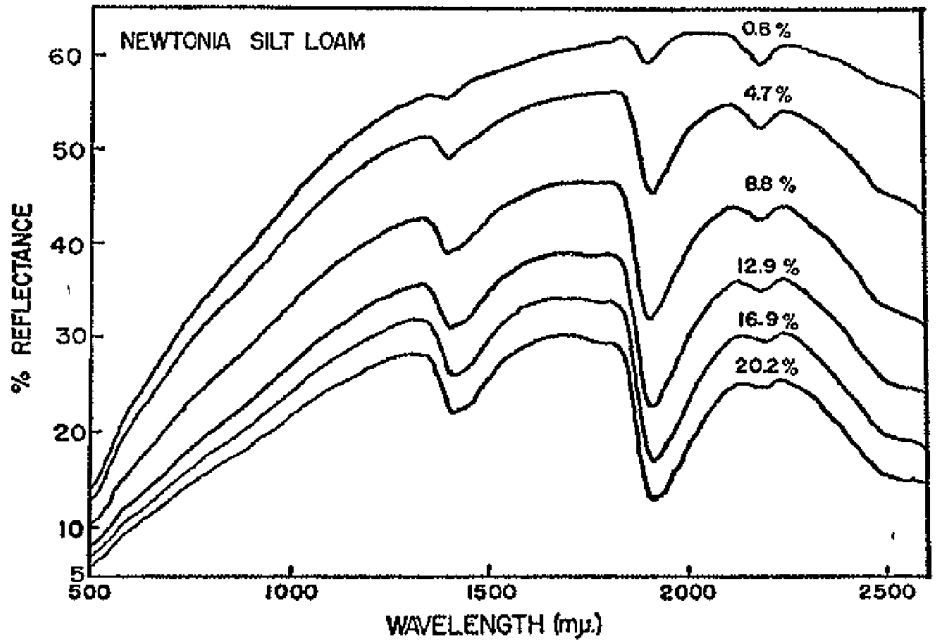

Figure 2.6 Percent Reflectance Versus Wavelength of Incident Radiation at Various Water Contents.

(Source: Bowers and Hanks, 1965)

Using a near infrared reflectance water meter with an integrating cylinder that has two interference bands at 1.8 and 1.94 μm, Kano et al. (1985) were able to detect soil water in clay and loam soils from 5% to 35%. Figures 2.7 and 2.8 show results normalized at 1.8 μm due to the reference wavelength of the NIR meter being selected at that wavelength.

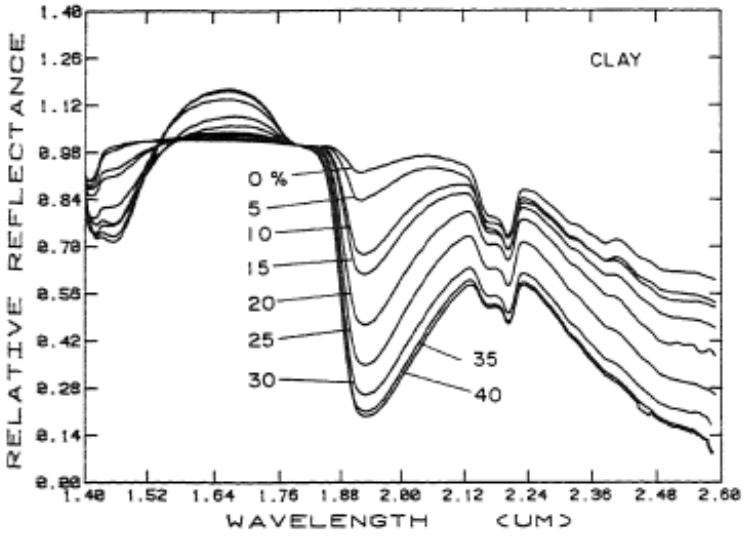

Figure 2.7 Near Infrared Reflectance of Clay at Various Soil Water Contents

(Source: Kano et al., 1985)

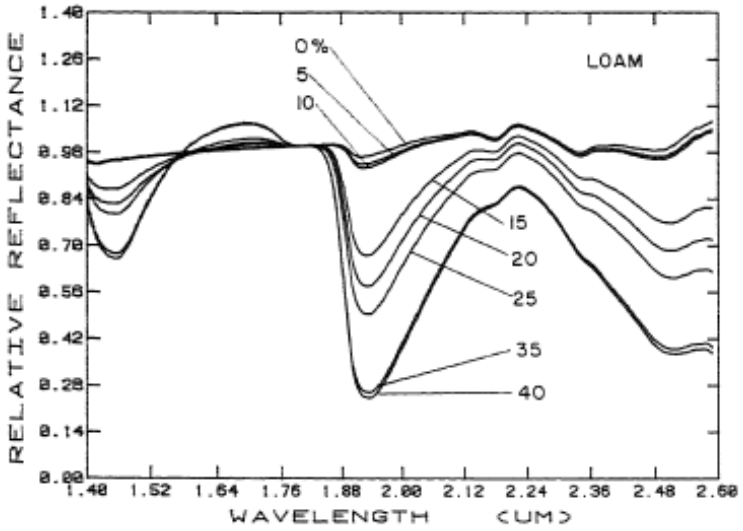

Figure 2.8 Near Infrared Reflectance of Loam at Various Soil Water Contents

(Source: Kano et al., 1985)

Using multispectral video imagery, Everitt et al. (1989) showed strong relationships between reflectance data and water content. Using five soil surface conditions; (1) wet smooth, (2) disked wet, (3) disked dry, (4) crusted dry, and (5) smooth dry, they were able to differentiate soil surface conditions. All tests were done with a Hidalgo fine sandy loam soil placed in stainless steel pans 8 cm deep as well as 9.1 m square field plots. Middle infrared reflectance of 1.45-2.0 µm showed the best correlation to soil water (r = 0.87 for field plots and r = 0.91 for pans), while visible and near infrared also showed high correlation to soil water.

Shih and Jordan (1992) used Landsat Thematic Mapper band 7, wavelength 2.08-2.35 µm, and observed that the response was inversely related to the qualitative soil water. Their results were from four land use types that included agricultural/irrigated, urban/clearing, forest/wetlands, and water.

Water strongly absorbs MIR centered on 1450, 1940, and 2500 nm and weak absorption bands near 970 and 1200 nm wavelengths in the NIR. Regions of intermediate absorption at 1650 and 2200 nm had also been used for remote sensing of water status in plants. Equivalent water thickness (EWT) in *Eucalyptus* species were shown to have the strongest correlation with reflectance in two semi-empirical indices, $(R_{850} - R_{2218})/(R_{850} - R_{1928})$ and $(R_{850} - R_{1788})/(R_{850} - R_{1928})$, where R represents the reflectance at the indicated wavelengths in nm (Datt, 1999).

2.2.2 Thermal Inertia

When soils contain high percentages of water, solar energy will be utilized for evaporation to dissipate energy into latent heat that in turn generates a cooling process for the top layer of soil. Moist soils also have greater thermal conductivity that transfers heat to the subsurface through conduction. This process is dependent upon soil thermal conductivity and temperature gradient (Moore et al., 1975). With these two processes combined, it becomes apparent that wet soils will remain cooler throughout a diurnal cycle than dry soils. A soil surface energy balance can be written as (McCumber and Pielke, 1981):

$$R_s + R_l - \sigma(T_g^4) + \rho L U_* Q_* + \rho C_p U_* T H_* - \rho_s C_s K_s (\partial T/\partial Z)_G = 0 \qquad \textbf{(2.5)}$$

where

R_s = incoming solar radiation (W/m^2)

R_l = incoming longwave radiation (W/m^2)

$\sigma(T_g)^4$ = blackbody radiation (W/m^2)

$\rho L U_* Q_*$ = turbulent latent heat flux (W/m^2)

$\rho C_p U_* T H_*$ = sensible heat flux (W/m^2)

$\rho_s C_s K_s (\partial T/\partial Z)_G$ = soil heat flux (W/m^2)

σ = Stefan-Boltzman constant (5.670×10^{-8} $W/m^2 \cdot K^4$)

T_g = soil surface temperature (K)

ρ = air density (kg/m^3)

ρ_s = soil density (kg/m^3)

L = specific latent heat (kJ/kg)

C_p = specific heat capacity ($J/g \cdot K$)

C_s = volumetric heat capacity ($J/m^3 \cdot K$)

K_s = thermal diffusivity ($W/m \cdot K$)

$(\partial T/\partial Z)_G$ = vertical temperature gradient (K/m)

$$U_* = \frac{K_0 \sqrt{U^2 + V^2}}{\ln \frac{Z}{Z_0} - I_1} \qquad \textbf{(2.6)}$$

$$TH_* = \frac{K_0\sqrt{X - X(Z_0)}}{0.74\ln\frac{Z}{Z_0} - I_2} \quad \textbf{(2.7)}$$

$$Q_* = \frac{K_0\sqrt{Q - Q(Z_0)}}{0.74\ln\frac{Z}{Z_0} - I_2} \quad \textbf{(2.8)}$$

where

K_0 = Von Karman's constant (0.35)

U,V = east-west and north-south components of wind speed, respectively (km/hr)

Q = atmospheric specific humidity (%)

TH = atmospheric potential temperature (°C)

Z = height, Z_0 is a turbulent roughness height (m)

I_1, I_2 = adjustments based on stability of the air

The thermal inertia approach to estimating soil surface water relies on the thermal properties of soil. The impedance of soil to temperature variations can be written as (Minacapilli et al., 2009):

$$P = \sqrt{\lambda\rho C} \quad \textbf{(2.9)}$$

where

P = soil impedance ($J/m^2 \cdot K \cdot s^{1/2}$)

λ = soil thermal conductivity ($W/m \cdot K$)

ρ = soil bulk density (kg/m^3)

C = soil heat capacity ($J/kg \cdot K$)

$$C = (\rho_b/\rho_s)C_s + \theta C_w \quad \textbf{(2.10)}$$

where

ρ_b = dry bulk density (kg/m^3)

ρ_s = density of solid phase (~2650 kg/m^3)

θ = volumetric soil water content (m^3/m^3)

C_s and C_w = heat capacities of soil and liquid phase ($J/kg \cdot K$)

Soil composition will cause the thermal conductivity of soil to vary significantly. No remote sensing technique can measure soil thermal inertia; however, models can be derived using the surface heat flux and diurnal temperature gains and losses (Minacapilli et al., 2009).

To measure soil water using surface temperature, it is essential to obtain meteorological variables (Wheeler and Duncan, 1984). Myhre and Shih (1990) used thermal infrared remote sensing to estimate soil water content in sandy soils. The technique involved measurement of the temperature difference between the air and surface along with meteorological variables. They used multiple linear regression analysis to create equations 2.8 and 2.9 to estimate soil water content.

$$WSWC = f(TD, SR, WS, RH) \quad \textbf{(2.11)}$$

$$WSWC = a_o + a_1TD + a_2SR + a_3WS + a_4RH \quad \textbf{(2.12)}$$

where

WSWC = weighted soil water content (%w.b.)

TD = soil surface to air temperature difference (°C)

SR = solar radiation (W/m^2)

WS = wind speed (m/s)

RH = relative humidity (%)

a_0, a_1, a_2, a_3, a_4 = regression coefficients

They measured soil water at depths of 15, 30, 60, and 90 cm and compared that to soil surface to air temperature difference on vegetated and bare soil surfaces. They got average coefficients of determination (R^2) of 0.62, 0.61, 0.63, and 0.60, respectively. Figure 2.9 shows selected sites and their regression coefficients (Myhre and Shih, 1990).

Site	Model* No.	Depth (m)	Regression coefficients a_0	a_1	a_2	a_3	a_4	r^2/R^2
S5 (trt TB)	1	0.15	12.27	-0.29				0.63
	2		10.59	-0.29	0.03			0.64
	3		12.09	-0.29	0.03	-0.02	-0.01	0.67
	4		12.25	-19.59				0.60
	1	0.30	12.56	-0.25				0.58
	2		12.29	-0.25	0.01			0.58
	3		13.05	-0.25	0.01	-0.01	-0.00	0.60
	4		12.51	-16.97				0.64
	1	0.60	13.38	-0.22				0.62
	2		12.94	-0.22	0.01			0.62
	3		14.53	-0.22	0.01	-0.01	-0.01	0.65
	4		13.34	-15.07				0.68
	1	0.90	14.38	-0.23				0.60
	2		12.19	-0.24	0.03			0.65
	3		13.73	-0.23	0.04	-0.02	-0.01	0.69
	4		14.50	-16.15				0.74
S6 (trt TG)	1	0.15	12.29	-0.40				0.76
	2		12.09	-0.40	0.00			0.76
	3		9.36	-0.32	0.03	-0.02	0.04	0.79
	4		12.11	-25.62				0.77
	1	0.30	12.47	-0.34				0.75
	2		11.73	-0.34	0.01			0.75
	3		12.66	-0.30	0.01	-0.02	-0.01	0.77
	4		12.34	-22.11				0.77
	1	0.60	12.80	-0.31				0.70
	2		14.57	-0.31	-0.03			0.72
	3		13.62	-0.27	-0.02	-0.01	0.01	0.73
	4		12.58	-18.65				0.78
	1	0.90	13.74	-0.27				0.65
	2		15.22	-0.27	-0.02			0.67
	3		13.34	-0.23	-0.01	-0.01	0.02	0.68
	4		13.53	-16.02				0.79

Site	Model* No.	Depth (m)	Regression coefficients a_0	a_1	a_2	a_3	a_4	r^2/R^2
S7 (trt G10)	1	0.15	13.59	-0.42				0.61
	2		15.32	-0.40	-0.03			0.63
	3		16.11	-0.43	-0.03	0.01	-0.01	0.64
	4		12.56	-21.26				0.57
	1	0.30	13.03	-0.32				0.58
	2		13.17	-0.32	-0.00			0.58
	3		15.07	-0.33	-0.01	0.01	-0.02	0.60
	4		12.35	-16.92				0.60
	1	0.60	13.24	-0.28				0.66
	2		12.31	-0.28	0.01			0.67
	3		11.96	-0.27	0.02	-0.00	0.01	0.68
	4		12.83	-16.25				0.66
	1	0.90	14.05	-0.32				0.71
	2		13.98	-0.32	0.00			0.71
	3		15.86	-0.32	-0.00	-0.01	-0.02	0.76
	4		13.39	-17.25				0.72
S8 (trt TB)	1	0.15	15.89	-0.41				0.62
	2		12.08	-0.42	0.06			0.67
	3		17.78	-0.43	0.05	-0.03	-0.06	0.75
	4		15.62	-27.20				0.66
	1	0.30	15.20	-0.33				0.66
	2		12.69	-0.34	0.04			0.70
	3		15.28	-0.33	0.04	-0.03	-0.02	0.77
	4		14.94	-21.62				0.69
	1	0.60	15.53	-0.29				0.71
	2		14.35	-0.30	0.02			0.72
	3		14.68	-0.28	0.02	-0.02	0.00	0.76
	4		15.08	-18.08				0.77
	1	0.90	16.15	-0.27				0.66
	2		14.43	-0.28	0.03			0.69
	3		14.22	-0.26	0.03	-0.02	0.01	0.73
	4		15.72	-16.86				0.73

Figure 2.9 Multiple Linear Regression Coefficients for Selected Sites

(Source: Myhre and Shih, 1990)

Alshikaili (2007) compared soil water estimations of clay versus sand and compacted versus non-compacted soils using the thermal inertia approach with meteorological variables. Alshikaili (2007) used a multiple linear regression model involving soil moisture content (SMC) as the dependent variable and differential temperature (T_d), solar radiation (SR), relative humidity (RH), and wind speed (WS) as the independent variables. Starting at 20% soil water content everyday with a soil depth of 6 cm, Alshikaili (2007) allowed the soil to dry outside from 10 A.M. to 8 P.M. The R^2 values for predicted soil water were 0.73 for compacted clay, 0.72 for non-compacted clay, 0.86 for compacted sand, and 0.83 for non-compacted sand. The research showed that method of thermal inertia and meteorological variables can provide non-destructive, inexpensive, and fast soil water content measurements (Alshikaili, 2007).

Sugiura et al. (2007) used low altitude thermal images from a helicopter to estimate soil water content in a bare rice paddy field measuring 125 m by 35 m. They took images at 10 A.M. and 3 P.M. on the same day from the helicopter at a height of 40 m at an oblique angle. They then matched the remotely sensed data with 32 ground samples taken at depths of 5 cm from the ground surface that were oven-dried to obtain actual soil water content. Since the image was taken at an oblique angle, each pixel is a different distance from the camera than any other pixel. Remotely sensed thermal imagery is greatly affected by atmospheric transmissivity, which is dependent on distance, ambient temperature, and humidity. They were able to correct the image using a table calculated by the algorithm of moderate resolution transmittance (MODTRAN) code. The raw data had R^2 values of 0.64 and 0.62 for the 10 A.M. and 3 P.M. images, respectively. The corrected data had R^2 values of 0.69 and 0.67. They also looked at the temperature difference between the images that had R^2 values of 0.42 in estimating soil water (Sugiura et al., 2007). Thermal images taken from high flying plane or satellite must do so on a clear day since thermal infrared is not able to penetrate through cloud cover that limits its usage to a degree (Hain et al., 2009).

A problem that arises when determining the temperature of soil through thermal infrared emittance is that soil emissivity is dependent on the soil water fraction. Since water has higher emissivity than bare soil, as the soil water fraction increases, the emissivity will increase as well. Research has shown that emissivity increases from 1.7% to 16% in sandy soils that have the highest variation of emissivity of any soils, in the 8.2-9.2 μm wavelength region of the thermal infrared spectrum. This is thought to be caused by water film on the soil particles diminishing reflectivity. That could result in errors of 0.1 to 2 K based on soil water influence alone on emissivity measured in that range (Mira et al., 2007).

Further research by Mira et al. (2010) using a variety of soil types showed a general increasing trend in emissivity with increasing soil water with water contents lower than field capacity. The relationship was once again strongest in the 8-9 μm range of sandy soils due to quartz or gypsum present in the soil, water adhering to soil grains, and decreasing reflectance. The 10-12 μm range showed little variation due to either soil water or soil type. Mira et al. (2010) also showed that knowing additional information about the soil composition (i.e., organic matter, quartz, and carbonate contents) improved the models. With known soil composition, it would be possible to estimate soil water with emissivity retrievals. Hulley et al. (2010) also

measured a 5% and 17% emissivity increase in two different sand sources at the 8.6 μm wavelength while measuring less than 3% in the 11-12 μm range.

2.2.3 Microwave (RADAR)

RADAR was first studied in 1922 by A.H. Taylor and L.C. Young along the Anacostia River near Washington, D.C. to detect distances of ships passing near by. There was much interest militarily to locate ships and planes. The acronym RADAR is derived from "**ra**dio **d**etection **a**nd **r**anging" and still holds even though microwave wavelengths are dominantly used instead of radiowaves (Jensen, 2007).

The use of the dielectric properties of soil has been used extensively to show soil water content in remotely sensed data. Most models that have described this relationship have been empirically and physically based. The dielectric constant ranges from 3 for dry soils to 30 for wet soils (Fernandez-Galvez, 2008). Water has a dielectric constant of roughly 80 (Jensen, 2007). The relationship is not linear however. If the water content is low, water molecules are held closely to the soil particle surface, restricting their ability to rotate freely and restricting the dipolar moment of free water. If the water content is high, on the other hand, water molecules can rotate freely. Finer soils (clays) have lower dielectric constants due to water being held in higher potential. Numerous soil dielectric models in literature do not take into account soil texture, which cannot be remotely sensed easily. Measurements in changes in soil water over time have more need than do absolute soil water content; however, large heterogeneous areas will require more exact measurements (Fernandez-Galvez, 2008).

Just how far RADAR can detect soil water into the soil profile depends on the wavelength used and water content. Wet soils reflect more RADAR energy than dry soils, but the RADAR energy will only penetrate a few centimeters into the soil. Dry soils can be penetrated to a depth equal to that of their wavelength, with active microwave systems able to penetrate several meters in very dry soils (Jensen, 2007).

Synthetic Aperture RADAR (SAR) can penetrate through cloud cover and yield information on the top 5 cm of bare soil using a frequency of 5.3 GHz in the C-band. The main soil characteristics that affect the level of RADAR backscatter are soil water through its dielectric properties and surface roughness. Kelly et al. (2003) showed that soil water can be predicted at the field level but cannot measure within field soil water variation at the 30 m pixel

size (Kelly et al., 2003). In order to apply a microwave system to a field or feedlot, the sensors would need to be 7 to 17 degrees off nadir. That means the sensor would have to be stationed high above ground level or used on an aircraft and flown at specified intervals (Wheeler and Duncan, 1984). If any vegetation is present on the soil surface, microwave remote sensing techniques become difficult and complex. When vegetation exceeds 1 Mg dry matter/ha, RADAR becomes limited in its ability to quantify soil water (Waring et al., 1995).

2.3 Application to Cattle Feedlots

When selecting a method for determining surface water in a feedlot it is important to understand the surface itself. A large commercial feedlot is designed to have a heterogeneous surface. Large mounds and wallows are placed in each pen to allow dry or wet areas to exist. Mounds are created to allow cattle to remain dry in the event of large precipitation events and wallows are created for cool, wet areas when temperatures rise. To characterize surface water accurately, one must realize the spatial variability present as shown in Figure 2.10.

Figure 2.10 Spatial Variability of Pen Surface Water in Cattle Feedlot

The most accurate remote sensing method for soil water is microwave or RADAR. However, the equipment is very expensive and since energy levels are low in this region of the electromagnetic spectrum, a large area is typically needed to gather enough energy to be detectable by the sensor. This method could be used in a satellite as part of a program to monitor water levels at the field level, but is not practical to a feedlot manager on a pen level basis.

Table 2.1 shows pros and cons for each remote sensing method that could be applicable to cattle feedlots. All remote sensing methods would have to be calibrated against the pen surface that is being measured. For this research, the thermal infrared method was selected due to its low cost and ground level approach.

Table 2.1 Remote Sensing Methodology

Remote Sensing Method	Pros	Cons
Near and Middle Infrared	• Accurate • Relatively inexpensive	• Very active portion of EM spectrum which could cause interference from organic material on surface
Thermal Infrared	• Sensors are inexpensive • Ground level, aircraft or satellite approach possible	• Not as precise as other methods • Measurement taken over time (not instantaneous)
Microwave	• Very accurate • Can measure large areas	• Very expensive • Can't measure variability less than 30 m pixel size due to low energy levels • Need tall standing structure or aircraft for sensors

CHAPTER 3 - Methods and Procedure

3.1 Introduction

A thermal inertia remote sensing approach was used in a laboratory setting, outdoor, and on a commercial feedlot. Laboratory experiments were conducted on two different soil compositions under a metal halide lamp. Each experiment consisted of running the lamp for 4 h and then allowing the soil to cool back to thermal equilibrium. Heating and cooling trends for 30 and 240 min were observed.

Outdoor testing took place on Kansas State University's (KSU) North Agronomy Research Farm. The site was selected due to a nearby weather station and being in an open area. Soil collected from a commercial cattle feedlot in Kansas was continuously weighed with a load cell as surface temperature, air temperature, solar radiation, wind speed, and relative humidity were collected. Soil depths of 5 and 10 cm were considered.

Testing on a commercial feedlot in Kansas was performed for four days to test the applicability of the thermal inertia remote sensing technique. The same meteorological variables were collected as the outdoor testing. Soil samples were collected daily at 1 P.M. from the pen surface for oven drying to determine surface water content.

3.2 Instrumentation and Testing Procedures

This section describes instrumentation for water content, artificial light and sunlight concentrations, soil surface temperature, air temperature, wind speed, and relative humidity.

3.2.1 Instruments

The CS300 Apogee Silicon Pyranometer, Figure 3.1, from Campbell Scientific is a silicon photovoltaic detector that measures sun plus sky radiation from 300 to 1100 nm. It can measure up to 2000 W/m^2. It is calibrated against a Kipp and Zonen CM21 thermopile pyranometer.

Figure 3.1 CS 300 Apogee Silicon Pyranometer

(Source: http://www.campbellsci.com)

A Control Company Traceable Dual-Range Light Meter, Figure 3.2, was used to measure artificial light levels from the metal halide lamp. It is calibrated against a tungsten light source. For a correct reading, the reading displayed must be corrected by multiplying with the following factors: mercury 1.05, fluorescent 0.91, and daylight 0.95.

Figure 3.2 Control Company Traceable® Dual-Range Light Meter

(Source: http://www.control3.com)

An SI-111 Precision Infrared Radiometer, Figure 3.3, was used to measure soil surface temperatures. It is composed of a thermopile that measures surface temperature and a thermistor that measures the sensor body temperature. It collects thermal radiation from the 8 to 14-µm wavelength range. The thermopile and thermistor output a millivolt signal that is used to

calculate target temperature using the Stefan-Boltzmann equation. This radiometer has an accuracy of ± 0.2°C from -10° to 65°C.

Figure 3.3 SI-111 Precision Infrared Radiometer

(Source: http://www.campbellsci.com)

The SI-111 radiometer has a 22° half angle field of view (FOV), as shown in Figure 3.4. The FOV is the half-angle of the apex of the cone formed by the target (cone base) and the detector (cone apex). The target is defined as the circle in which 98% of the radiation detected by the senor is being emitted. Typically 95-98% of the thermal infrared signal is from the field of view while 2-5% is from the outside the field of view.

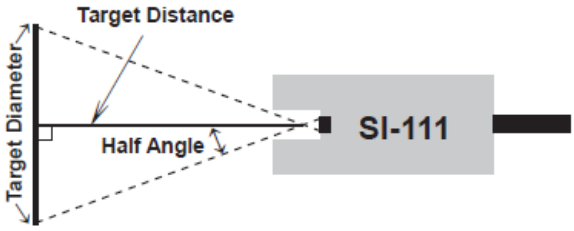

Figure 3.4 SI-111 Precision Infrared Radiometer Field of View Diagram

(Source: http://www.campbellsci.com)

A Stevens Hydra Probe II, Figure 3.5, was used for continuous measurement of soil water. It is able to calculate soil water, conductivity, salinity, and temperature. The Hydra Probe has four metal rods that extend from the 25-mm base plate that are 45 mm long and 3 mm in diameter. The head of the probe houses the circuit boards, microprocessors, and all the electrical equipment. From there, electromagnetic waves are transmitted at radio frequency from the outer

tines and received by the center tine. The Hydra Probe is able to achieve ±0.03 water fraction by volume (wfv) (m^3/m^3) on a wet basis accuracy and ±0.003 wfv precision.

Figure 3.5 Stevens Hydra Probe II Soil Water Sensor (SDI-12)

(Source: http://www.stevenswater.com)

The Hydra Probe has four calibration curves that it can use. The curves are polynomials that have unique real dielectric constants and several coefficients. The four settings are Sand, Silt, Clay, and Loam. The default setting and the best setting for most soils is the Loam setting. It is applicable for Loam, Clay Loam, Silty Clay Loam, Silt Loam, Sandy Loam, Sandy Clay Loam, Sandy Clay, and Silty Clay textures. Figure 3.6 shows where the loam setting is applicable on the soil texture triangle.

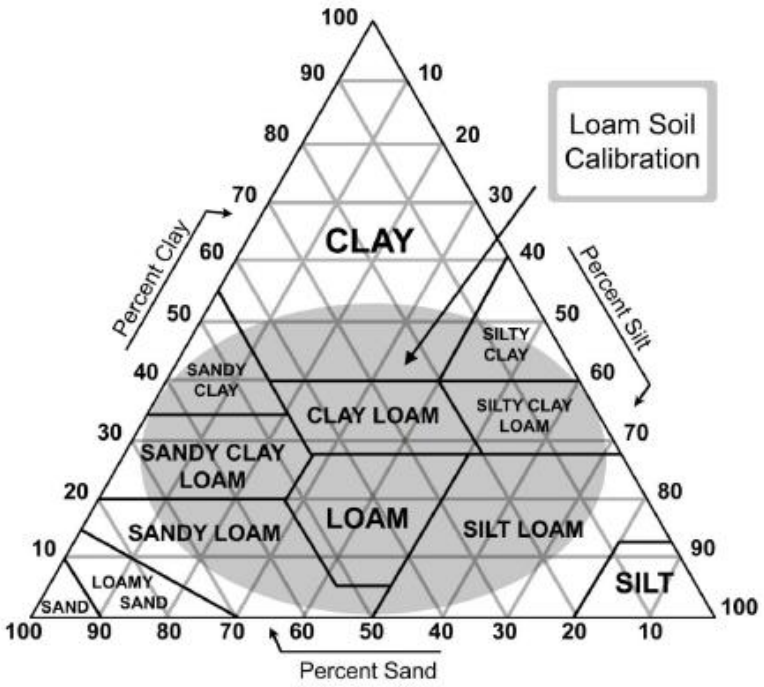

Figure 3.6 Loam Soil Calibration

(Source: http://www.stevenswater.com)

In order for the probe to work properly, the base plate must be flush to the soil in order for good contact. If there is an air gap, the Hydra Probe signal will average the gap into the measurement and result in errors.

Campbell Scientific CR800, Figure 3.7, and 21X, Figure 3.8, dataloggers were used. The CR800 supported the thermal infrared radiometer, soil water probe, one thermocouple and pyranometer while the 21X contained 6 thermocouples and the load cell.

Figure 3.7 CR800 Datalogger

(Source: http://www.campbellsci.com)

Figure 3.8 21X Datalogger

(Source: http://www.campbellsci.com)

Air temperature, relative humidity, and wind speed were all collected by Kansas State University Research and Extension's weather station. Air temperature and relative humidity used a HMP50 sensor at a height of 1.5 m while wind speed was measured by a met-one 3-cup anemometer at a height of 2 m.

A MLP-50 load cell, Figure 3.9, was purchased from Transducer Techniques, Inc. Since the load cell is only calibrated in compression, calibration had to be done in tension.

Figure 3.9 MLP-50 Load Cell

(Source: http://www.transducertechniques.com)

Small weights were used to create the linear calibration curve. The string that was connected to hold the weights was 16.22 g. One hundred and 1000 g weights were used in combination to get nine points. The heaviest weight achieved was 2216.22 g, which is only $1/10^{th}$ of the total capacity. Figure 3.10 shows the linear curved derived from calibration.

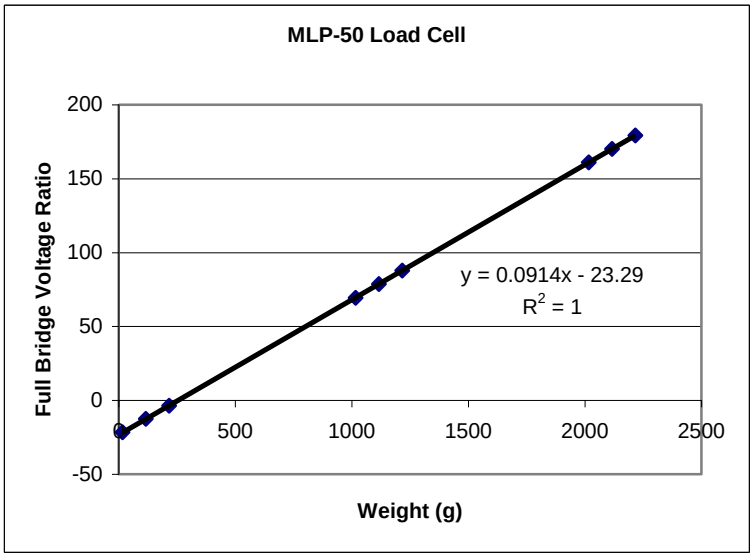

Figure 3.10 Tension Calibration Curve of Load Cell

Reversing the axes of the calibration curve will put the weight as the dependent variable and allow for simple computation once the reading of the voltage ratio is known from the datalogger. Figure 3.11 shows the linear curve used in calculating weighted soil water content.

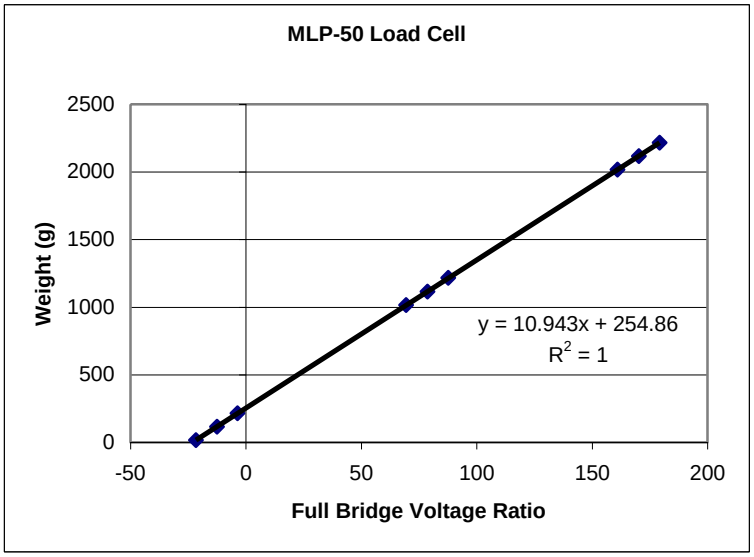

Figure 3.11 Reverse Tension Calibration Curve of Load Cell

3.2.2 Laboratory Testing

To get the light concentration high enough to levels similar to natural sunlight, aluminum foil was used to focus the light onto the soil samples, as seen in Figure 3.12. This approach was used to keep the soil far enough away from the heat of the lamp so the only energy source is the radiation. The room typically had temperatures ranging from 20-29°C so it was necessary to look at temperature gain/loss instead of absolute temperatures.

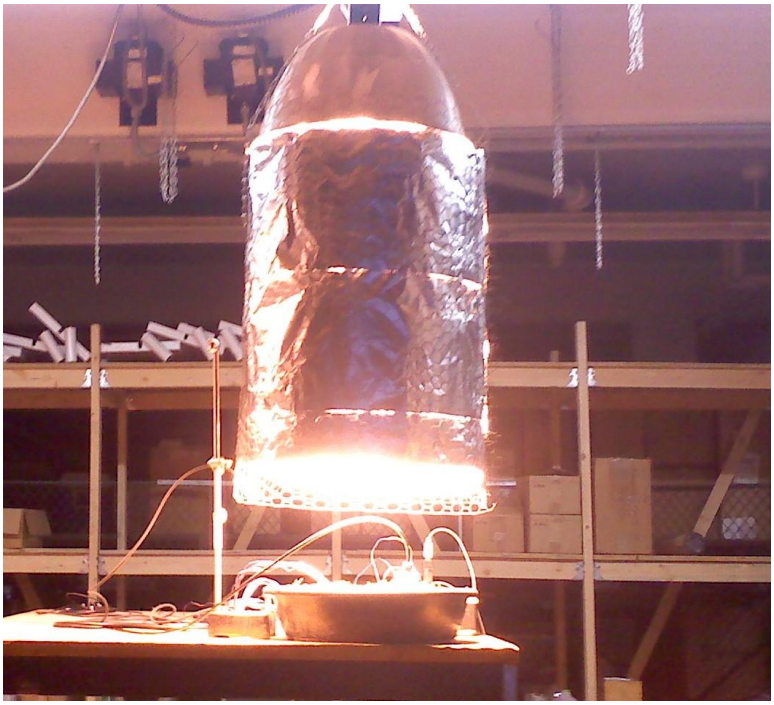

Figure 3.12 Indoor Laboratory Setup

The diameter of the metal covering on the lamp fixture was 47 cm. The aluminum foil was 68 cm in height and was able to overlap the entire surface of the soil which was 41 cm in diameter. There was a 23-cm gap between the bottom of the aluminum foil and the soil surface. Although the artificial light was constant, it was not uniform. Light intensity was highest in the center and decreased towards the edges. The center of soil surface had the highest light intensity of 507 W/m^2 using the CS300 Apogee Silicon Pyranometer. The perimeter of the soil surface had an average of 220 W/m^2. The center light intensity was also measured with a Traceable® Dual-Range Light Meter from Fisher Scientific at 106,500 lux. The perimeter of the soil surface measured 56,100 lux. The light meter has a calibrated range up to 50,000 lux, but the proportion of the center position to the perimeter was in line with the CS300 Apogee Silicon Pyranometer. Light conditions were thus similar to a sunny winter day in Kansas. Precaution was taken not to adjust the position of the infrared thermometer, shown in Figure 3.13, due to uneven heating that could have taken place on the soil surface.

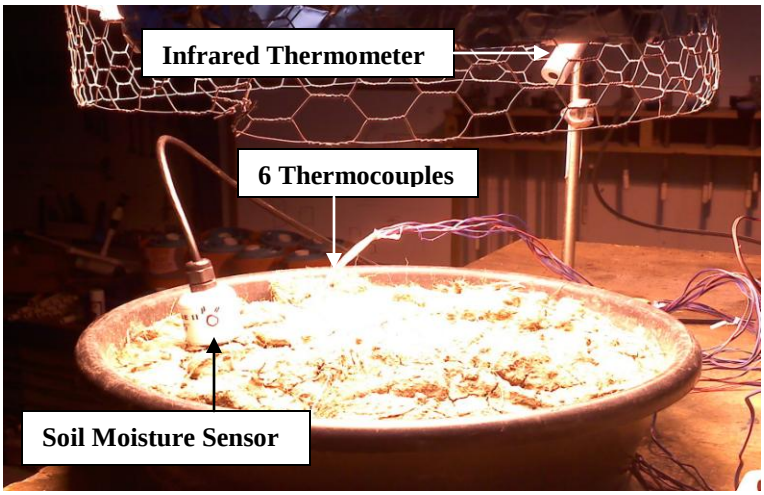

Figure 3.13 Soil Surface during Heating

The first soil type used was collected at the North Agronomy Research Farm. According to the USDA Web Soil Survey it was a Smolan silt loam. The second soil type was collected from a Texas cattle feedlot that was dried and sieved to remove large clods. Testing at the KSU Soil Testing Lab showed it had 66% sand, 12% silt, and 22% clay with 8% organic matter. Soil water was measured by the Stevens Hydra Probe II for the Smolan silt loam and by oven drying for the dried feedlot soil. A sample of 6 to 17 g was collected at the beginning of the heating period for the dried manure, which is the same time soil water was determined for the silt loam. Table 3.1 shows a summary of the instruments used for laboratory testing.

Table 3.1 Laboratory Testing Instruments

Parameter	**Instrument/Method**	**Sampling Frequency**	**Sampling Duration**	**Accuracy**
Water Content	SDI-12 Hydra Probe	5 min	5 min	± 0.03 wfv
	Oven Drying	Once per run	24 h	
Soil Surface Temperature	SI-111 Infrared Radiometer	5 min	< 1 s	± 0.2°C
Air Temperature	Thermocouple	5 min	< 1 s	± 1°C
Light Intensity	CS 300 Pyranometer	Once	< 1 s	± 5% for daily total radiation
	Dual-Range Light Meter	Once	< 1 s	± 5% full scale plus 2 digits

3.2.3 Outdoor Testing

Outdoor experiments were conducted at the KSU North Agronomy Research Farm. The experimental setup, Figure 3.14, consisted of obtaining a soil sample that was continuously weighed with a 22.7-kg load cell. The CR800 datalogger ran the thermal infrared thermometer, pyranometer, and one thermocouple for air temperature. The 21X ran the load cell and six thermocouples. The units for measurement were degrees Celsius for soil surface and air temperature, watts per square meter for solar radiation, and percentage for both weighted soil water content and relative humidity. Data were collected from April 27th to June 30th, 2010 for the 10-cm depth and from July 2nd to September 5th, 2010 for the 5-cm depth.

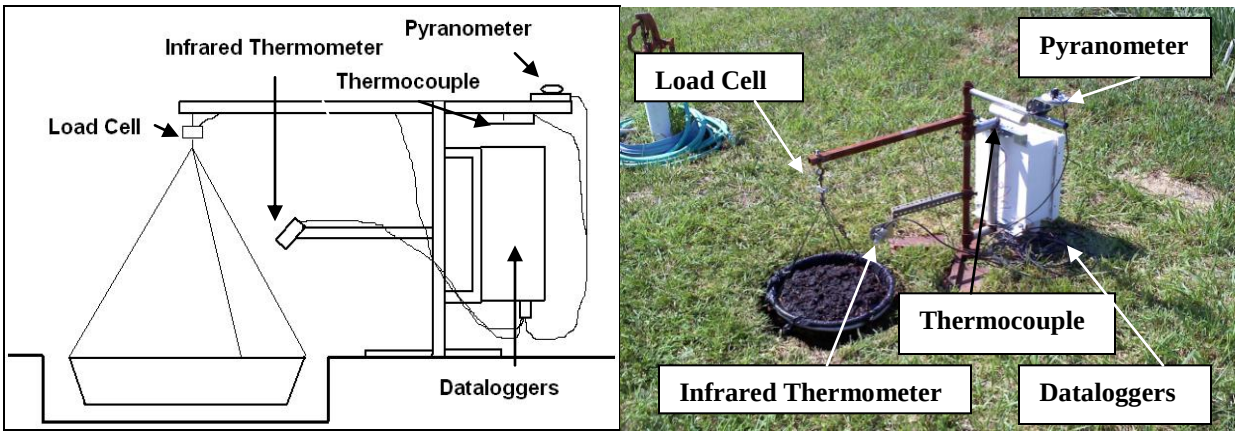

Figure 3.14 Experimental Setup at the North Agronomy Research Farm: (a) Schematic Diagram (b) Setup

A sample soil from a pen in a commercial cattle feedlot in Kansas was used. According to the USDA Web Soil Survey it is a Pratt loamy fine sand. Soil testing indicated that it was 61% sand, 21% silt, and 18% clay with 7.1% organic matter content. Taking an oven-drying soil water sample before and after testing, the 10-cm soil depth had an initial water content of 46.1% wet basis. A starting total weight of 10,339 g was composed of 5568 g of dry soil and 4771 g of water. The 5-cm soil depth had an initial soil water content of 50.3% wet basis. The total weight of 5688 g was composed of 2828 g of dry soil and 2860 g of water. It was assumed that all weight losses and gains were due only to changes in water weight. Wind erosion was considered negligible. With sufficient rain events through July, the soil did not need added water until August to increase the number of drying cycles and provide the regression models with more data points in higher soil water contents. Table 3.2 shows a summary of the instruments used in outdoor testing.

Table 3.2 Outdoor Testing Instruments

Parameter	Instrument/Method	Sampling Frequency	Sampling Duration	Accuracy
Water Content	MLP-50 Load Cell	5 min	< 1 s	± 0.1% of rated output
	Oven Drying	Initial, Final	24 h	
Soil Surface Temperature	SI-111 Infrared Radiometer	5 min	< 1 s	± 0.2°C
Air Temperature	Thermocouple	5 min	< 1 s	± 1°C
	HMP50 Sensor	1 h	1 h	± 0.5°C
Solar Radiation	CS 300 Pyranometer	5 min	< 1 s	± 5% for daily total radiation
Wind Speed	Met-one 3-cup Anemometer	1 h	1 h	± 0.11 m/s or 1.5 %
Relative Humidity	HMP50 Sensor	1 h	1 h	±3%, 0 to 90% range; ±5%, 90 to 98% range

3.2.4 Feedlot Testing

Feedlot testing was conducted September 19-25, 2010. The feedlot has approximately 30,000 head of cattle in a total pen area of 59 ha. A small portion of a feedlot pen was fenced off to prevent cattle from tampering with the instruments. Surface temperature and solar radiation were collected on-site, as shown in Figure 3.15. Air temperature, wind speed, and relative humidity were collected at a nearby weather station. The soil surface was near the location where the soil sample for the outdoor testing was collected. According to the USDA Web Soil Survey it is a Pratt loamy fine sand, which accounts for 55% of the total feedlot surface soil. Soil testing indicated that it was 56% sand, 22% silt, and 22% clay with 4.2% organic matter content. Soil samples were collected daily at 1 P.M. for oven drying to determine soil surface water content in the top layer.

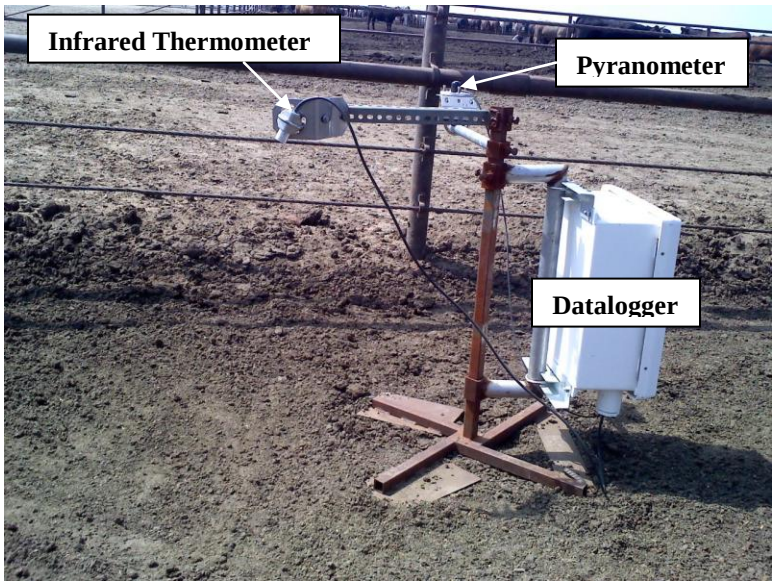

Figure 3.15 Feedlot Setup

3.3 Data Analysis

3.3.1 Laboratory Testing

With a constant light source and indoor conditions, remotely sensing soil water with the thermal inertia approach becomes solely dependent on the water content in the soil. Air temperature in the room did fluctuate by several degrees Celsius so it was important to analyze temperature differences. Analysis was done using 30 and 240-min temperature gain and losses. This was selected to see how quickly soil water could be predicted. This method of measurement could become more desirable if only a short time frame is needed to accurately measure water content. Due to changing water contents during heating, the water content was determined when the lamp was first turned on to start the run.

3.3.2 Outdoor Testing

Stepwise multiple linear regressions were performed for both the 5 and 10-cm soil depths. Using stepwise regressions the strength of each meteorological variable into the models could be seen. Using as few as possible parameters in remotely measuring the water content makes the method simpler and more readily accessible for application. Weighted water content was selected at 1 P.M. for each day regardless of the method used.

3.3.3 Emissivity Analysis

For both the indoor and 10-cm outdoor depth, emissivity testing was done to see if the soil surface temperature measured by the infrared thermometer was accurate for dry and wet soil surfaces. If large changes were seen, necessary adjustments will need to be taken for accurate modeling. Data points were collected when all 6 thermocouples evenly spaced in the 10-cm soil profile had identical temperature measurements. All points were obtained overnight throughout the testing period when there was no soil temperature gradient and soil temperatures were near air temperature. Since the thermocouples have an accuracy of ± 1°C and the infrared thermometer's accuracy is ± 0.2°C, precise emissivity values will deviate slightly from true values. However, an overall trend should be able to be seen in the data set.

CHAPTER 4 - Results and Discussion

4.1 Laboratory Testing

4.1.1 Smolan Silt Loam

Both the 30-min temperature gain and loss equations were fitted as power functions with R^2 values of 0.89 and 0.91, respectively, in predicting soil water by percentage volume. Figure 4.1 shows 30-min temperature gain had a minimum gain of 11.1°C with high soil water contents and a maximum gain of 24.3°C for low soil water contents. Using 30-min temperature loss, high soil water contents lost a minimum of 9.8°C while low soil water contents lost a maximum of 23.2°C.

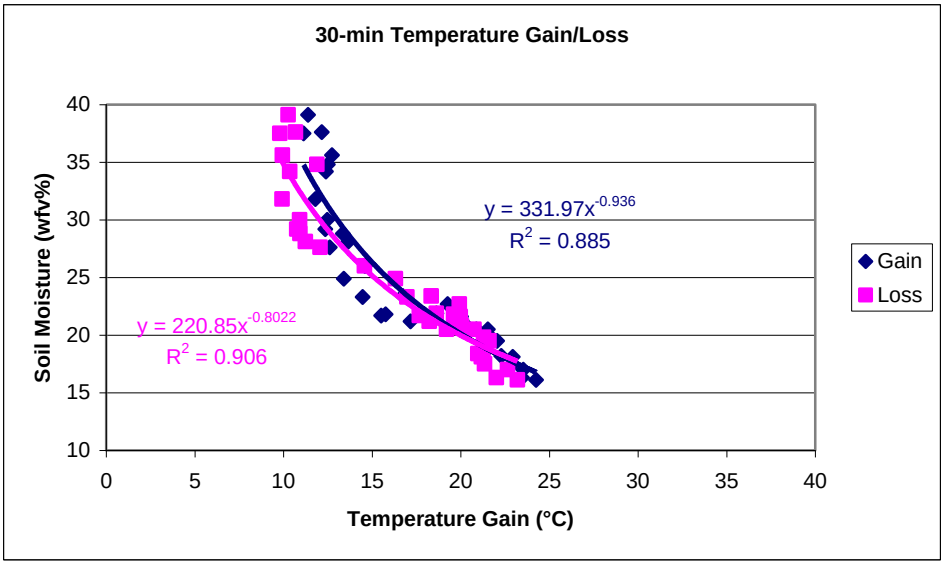

Figure 4.1 Smolan Silt Loam 30-min Temperature Gain/Loss

Figure 4.2 shows 240-min temperature gain had a minimum gain of 14.1°C with high soil water contents and a maximum gain of 33.1°C for low soil water contents. Using 240-min temperature loss, high soil water contents lost a minimum of 9.8°C while low soil water contents lost a maximum of 23.2°C

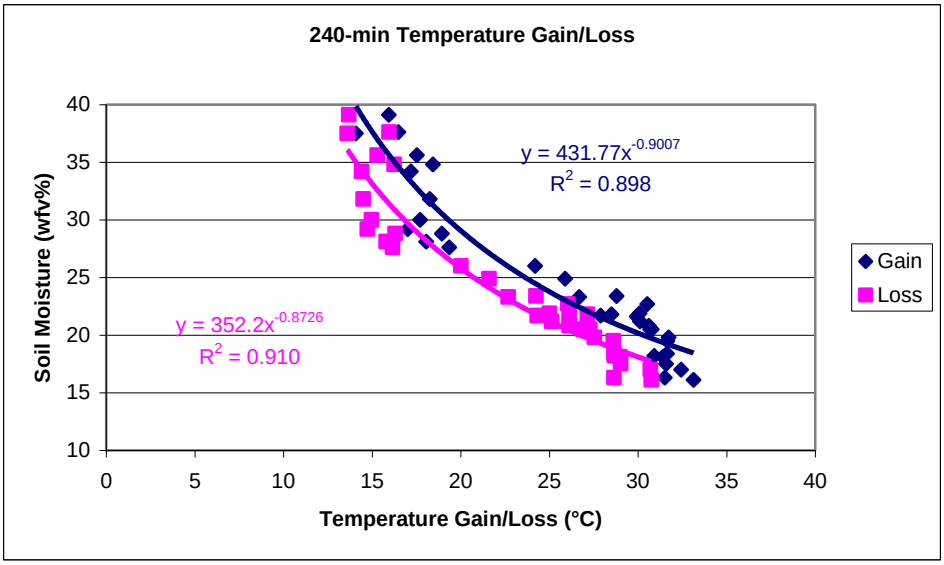

Figure 4.2 Smolan Silt Loam 240-min Temperature Gain/Loss

4.1.1.1 Emissivity Testing

The change in emissivity of the Smolan silt loam under dry and wet conditions was small using the SI-111 Precision Infrared Radiometer. When the soil was dry, the infrared radiometer overestimated the soil temperature as much as 0.59°C and when the soil was wet, the infrared radiometer underestimated the soil temperature as much as 1.37°C, as shown in Figure 4.3. These results run counter to literature (Mira, et al., 2007) since wet soils have higher emissivity and should have readings closer to the actual temperature than dry soils.

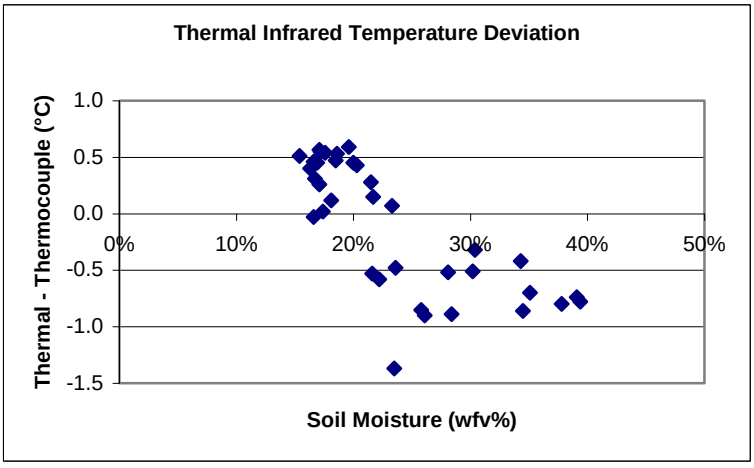

Figure 4.3 Smolan Silt Loam Thermal Infrared Temperature Deviation

4.1.2 Dried Feedlot Soil

Figure 4.4 shows 30-min temperature gains varying from 10.6°C under high water contents to 25.8°C for low water contents. Thirty minute temperature losses ranged from 12.1°C for high water contents to 26.2°C for low water contents. Both equations were best fitted as linear functions with R^2 values of 0.83 for gain and 0.82 for loss.

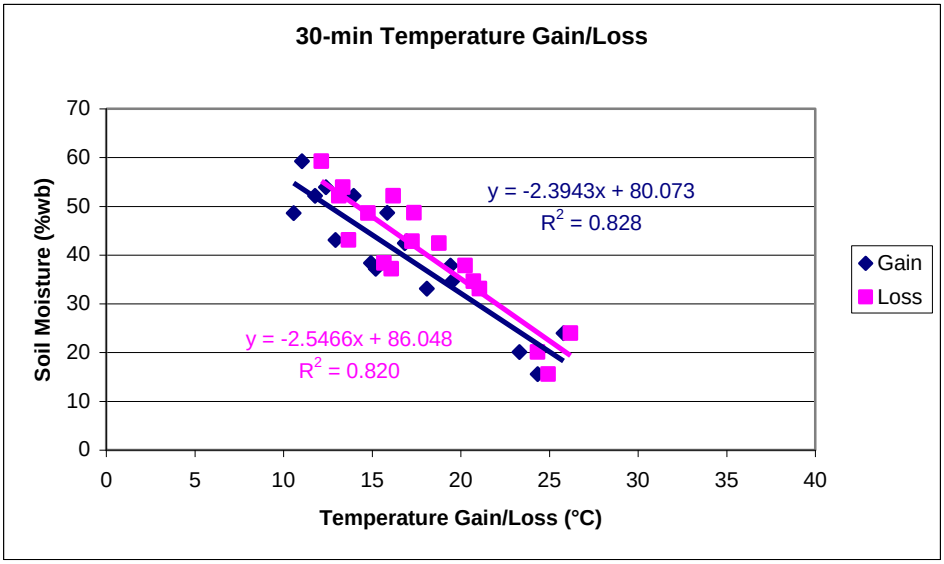

Figure 4.4 Dried Feedlot Soil 30-min Temperature Gain

Figure 4.5 shows 240-min temperature gains ranging from 17.4°C for high water contents to 34.4°C for low water contents. Figure 4.5 shows 240-minute temperature losses ranged from 16.1°C for high water contents to 31.6°C for low water contents. Both equations were best fitted as linear functions with R^2 values of 0.83 for gain and 0.82 for loss.

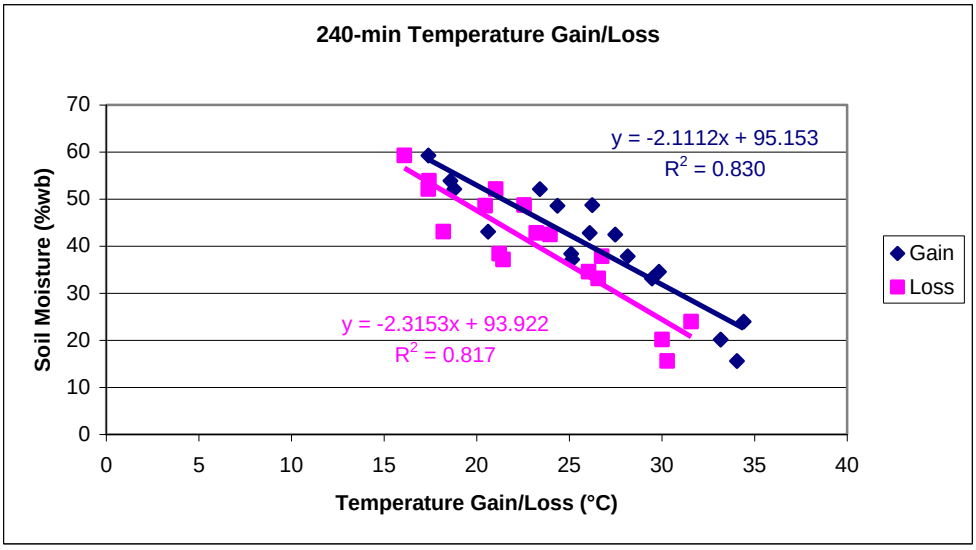

Figure 4.5 Dried Feedlot Soil 240-min Temperature Gain/Loss

4.2 Outdoor Testing

Days were not used in data analysis if it rained during daylight hours due to changing weighted soil water content and cooling of the soil surface from rainfall. The 10-cm soil depth had a total of 49 useable days while the 5-cm soil had a total of 54 useable days. For further analysis, selected dates were used where no fluctuations in solar radiation or at most very little fluctuation. This can be seen in Table 4.1 where standard deviation for solar radiation decreased from 281 to 118 W/m^2 for the 10-cm depth and from 230 to 112 W/m^2 for the 5-cm depth. This was performed to control for variations in solar energy input into the soil. The 10-cm depth had 35 days while the 5-cm depth had 45 days.

Table 4.1 Statistical Summary of Meteorological Variables

			10 cm				5 cm			
	Parameter	Units	**Min**	**Mean**	**Max**	**STDV**	**Min**	**Mean**	**Max**	**STDV**
All Data	**Water Content**	%	36.3	45.3	50.8	3.5	3.5	26.9	54.4	13.1
	Air Temp	°C	13.4	25.2	34.0	6.0	22.6	31.2	37.7	3.5
	Soil Surface Temp	°C	14.1	40.7	55.3	10.8	22.7	48	63.1	9.6
	Solar Radiation	W/m^2	80	839	1180	281	44	802	1145	230
	Wind Speed	m/s	1.5	3.7	7.3	1.4	1.6	3.1	5.2	0.9
	Relative Humidity	%	27.2	55.0	93.8	14.8	29.3	55.1	86.1	12.6
Select Data	**Water Content**	%	36.3	44.9	50.6	3.4	5.8	25.0	50.8	11.8
	Air Temp	°C	14.8	26.1	34.0	5.5	23.7	31.9	37.7	3.1
	Soil Surface Temp	°C	27.8	44.6	55.3	8.2	29.2	50.8	63.1	7.5
	Solar Radiation	W/m^2	519	969	1180	118	401	882	1145	112
	Wind Speed	m/s	1.6	3.8	7.3	1.6	1.7	3.2	5.2	1.0
	Relative Humidity	%	27.2	49.8	69.9	11.6	29.3	51.9	70.1	10.0

Multiple linear regressions were performed using weighted soil water content (WSWC) as the response and soil surface to air temperature difference (TD), solar radiation (SR), wind speed (WS), and relative humidity (RH) as the predictors. First regressions performed used a single measurement in time at 1 P.M. to predict soil water. Second regressions were performed using the change in temperature from 6 A.M. to 1 P.M. as a predictor. Third regressions performed used the point in time where the soil surface temperature was at its daily peak. This point varied throughout the afternoon depending on the weather conditions for a particular day.

Multiple linear regressions were also performed using an alternate form of equation (2.12). As mentioned earlier,

$$WSWC = a_o + a_1TD + a_2SR + a_3WS + a_4RH \quad \textbf{(4.1)}$$

Equation (2.12) uses the four known variables as the predictors and the unknown variable, WSWC, as the response. While this method will pick up relationships among all four predictors, the physical relationship is not justified. There is a direct physical relationship between TD and WSWC, but no relationships between solar radiation, wind speed, and relative humidity (away from the surface) to WSWC. Equation (4.2) was generated to show the true physical relationship.

$$TD = a_0 + a_1SR + a_2WSWC + a_3WS + a_4RH \quad \textbf{(4.2)}$$

where

TD = soil surface to air temperature difference (°C)

SR = solar radiation (W/m^2)

WSWC = weighted soil water content (%)

WS = wind speed (m/s)

RH = relative humidity (%)

Equation (4.2) allows for each of the predictors to accurately describe the response. As solar radiation increases, so will the soil surface to air temperature difference which results in a positive correlation. As weighted soil water content is increased the soil surface to air temperature difference will decrease due to increased soil thermal inertia and latent heat losses to

evaporation which results in a negative correlation. Increased wind speeds will help dissipate heat from the soil surface due to convective cooling. As wind speeds increase, the surface soil to air temperature difference lessens resulting in a negative correlation. A high relative humidity means the air has a higher vapor pressure and thus cannot evaporate water in the soil as quickly, reducing evaporation and transfer of latent heat. This was expected to have a positive correlation with soil surface to air temperature difference.

4.2.1 Ten cm Soil Depth

Using the equation (2.12), stepwise multiple linear regression tables were created to analyze the strength of each of the four predictors. Table 4.2 shows R^2 values for the three thermal inertia methods used on all 49 days. Using the soil surface to air temperature difference at 1 P.M., an R^2 value of 0.35 was achieved. Soil surface to air temperature gain from 6 A.M. to 1 P.M. achieved an R^2 value of 0.34. The peak soil temperature method achieved an R^2 value of 0.38.

Table 4.2 Ten cm Multiple Linear Regression Coefficients for All Data

	Regression Coefficients					
		TD	SR	WS	RH	
	a_0	a_1	a_2	a_3	a_4	R^2
Difference	48.6	-0.212				0.193
	46.1	-0.380	0.00600			0.302
	47.5	-0.429	0.00760	-0.523		0.339
	44.9	-0.379	0.00750	-0.471	0.0311	0.346
Gain	48.8	-0.190				0.195
	46.5	-0.342	0.00610			0.307
	47.6	-0.372	0.00720	-0.425		0.332
	45.8	-0.338	0.00710	-0.392	0.0224	0.335
Peak Soil Temp	51.4	-0.299				0.295
	47.3	-0.385	0.00640			0.351
	48.3	-0.425	0.00790	-0.424		0.377
	51.4	-0.479	0.00760	-0.471	-0.0312	0.385

Table 4.3 shows the results for the 35 select days. Small gains were seen in predictive strength of the models. R^2 values were as follows: temperature difference at 1 P.M., 0.35; temperature gain from 6 A.M. to 1 P.M., 0.37; and peak soil temperature, 0.38.

Table 4.3 Ten cm Multiple Linear Regression Coefficients for Select Data

	Regression Coefficients					
		TD	SR	WS	RH	
	a_0	a_1	a_2	a_3	a_4	R^2
Difference	50.7	-0.316				0.266
	45.4	-0.348	0.0062			0.310
	46.1	-0.396	0.0080	-0.428		0.341
	49.6	-0.454	0.0078	-0.505	-0.0395	0.352
Gain	51.2	-0.286				0.275
	45.8	-0.315	0.0063			0.320
	46.4	-0.345	0.0076	-0.338		0.340
	53.3	-0.453	0.0074	-0.478	-0.0758	0.372
Peak	51.0	-0.274				0.203
Soil Temp	38.8	-0.309	0.0136			0.346
	39.8	-0.341	0.0143	-0.250		0.358
	44.3	-0.433	0.0150	-0.367	-0.0591	0.381

Using equation (4.2), which uses TD as the response, all three models saw improved strength as shown in Table 4.4 and Table 4.5. R^2 values for all 49 days as shown in Table 4.4 are as follows: temperature difference at 1 P.M., 0.79; temperature gain from 6 A.M. to 1 P.M., 0.81; and peak soil temperature, 0.76.

Table 4.4 Revised 10-cm Multiple Linear Regression Coefficients for All Data

	Regression Coefficients					
		SR	WSWC	WS	RH	
	a0	a1	a2	a3	a4	R^2
Difference	-0.3	0.0188				0.523
	35.7	0.0179	-0.780			0.665
	38.9	0.0194	-0.777	-1.24		0.720
	40.5	0.0144	-0.510	-1.18	-0.178	0.794
Gain	0.8	0.0211				0.525
	41.4	0.0202	-0.880			0.668
	44.5	0.0215	-0.878	-1.17		0.707
	46.6	0.0151	-0.532	-1.09	-0.231	0.805
Peak	-0.4	0.0228				0.305
Soil Temp	41.9	0.0207	-0.893			0.544
	43.6	0.0223	-0.867	-1.19		0.615
	50.9	0.0128	-0.619	-1.07	-0.199	0.759

Table 4.5 shows the results for the 35 select days. R^2 values were as follows: temperature difference at 1 P.M., 0.66; temperature gain from 6 A.M. to 1 P.M., 0.72; and peak soil temperature, 0.68.

Table 4.5 Revised 10-cm Multiple Linear Regression Coefficients for Select Data

	Regression Coefficients					
		SR	WSWC	WS	RH	
	a_0	a_1	a_2	a_3	a_4	R^2
Difference	7.5	0.0114				0.060
	45.1	0.0133	-0.879			0.347
	44.9	0.0170	-0.846	-1.29		0.474
	52.4	0.0107	-0.627	-1.30	-0.224	0.665
Gain	9.6	0.0128				0.060
	52.5	0.0150	-1.00			0.357
	52.3	0.0185	-0.970	-1.22		0.447
	62.3	0.0101	-0.676	-1.24	-0.300	0.721
Peak Soil Temp	13.8	0.0088				0.023
	44.9	0.0186	-0.902			0.295
	44.9	0.0198	-0.816	-1.30		0.432
	50.0	0.0165	-0.611	-1.26	-0.244	0.677

Large differences in the strength of the models were seen between equations (2.12) and (4.2).

4.2.1.1 Emissivity Testing

The change in emissivity of the feedlot soil under dry and wet conditions was small using the SI-111 Precision Infrared Radiometer. Points were taken when all six thermocouple readings were identical or near identical. When the soil was dry, the infrared radiometer underestimated the soil temperature as much as 3.25°C and when the soil was wet, the infrared radiometer underestimated the soil temperature as little as 0.04°C. These results agree with literature in that wet soils have higher emissivity and should have readings closer to the actual temperature than dry soils. Figure 4.6 shows the scatter plot of the results. The soil water content (%w.b.) is the average soil water throughout the 10-cm layer, not soil surface water.

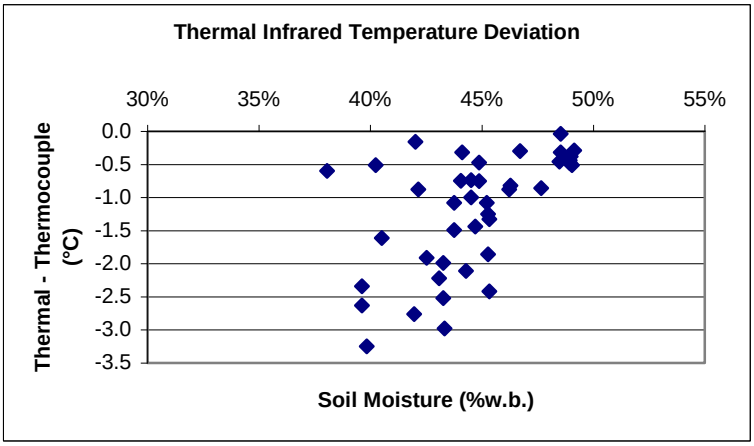

Figure 4.6 Feedlot Soil Thermal Infrared Temperature Deviation

4.2.2 Five cm Soil Depth

Using the equation (2.12) for the 54 useable days for the 5 cm soil depth, R^2 values as seen in Table 4.6 were as follows: temperature difference at 1 P.M., 0.58; temperature gain from 6 A.M. to 1 P.M., 0.56; and peak soil temperature, 0.59.

Table 4.6 Five cm Multiple Linear Regression Coefficients for All Data

	Regression Coefficients					
		TD	SR	WS	RH	
	a_0	a_1	a_2	a_3	a_4	R^2
Difference	42.6	-0.94				0.277
	29.3	-1.49	0.0281			0.426
	41.7	-1.69	0.0339	-4.40		0.519
	16.5	-1.63	0.0402	-3.75	0.309	0.585
Gain	43.9	-0.85				0.266
	30.6	-1.45	0.0317			0.440
	44.5	-1.70	0.0390	-4.84		0.550
	31.7	-1.61	0.0407	-4.41	0.150	0.564
Peak	50.6	-1.14				0.291
Soil Temp	27.9	-1.67	0.0389			0.425
	51.1	-2.04	0.0441	-6.22		0.573
	41.6	-1.93	0.0427	-5.84	0.137	0.589

Using equation (2.12) for the 45 useable select days for the 5-cm soil depth, R^2 values as seen in Table 4.7 were as follows: temperature difference at 1 P.M., 0.67; temperature gain from 6 A.M. to 1 P.M., 0.65; and peak soil temperature, 0.54.

Table 4.7 Five cm Multiple Linear Regression Coefficients for Select Data

	Regression Coefficients					
		TD	SR	WS	RH	
	a_0	a_1	a_2	a_3	a_4	R^2
Difference	46.6	-1.14				0.338
	6.1	-1.33	0.0500			0.553
	26.2	-1.59	0.0456	-3.63		0.618
	16.0	-1.63	0.0414	-3.65	0.286	0.674
Gain	50.3	-1.13				0.351
	11.0	-1.30	0.0488			0.557
	36.5	-1.62	0.0435	-4.33		0.645
	31.4	-1.59	0.0417	-4.21	0.112	0.654
Peak	50.7	-1.16				0.294
Soil Temp	24.9	-1.46	0.0363			0.378
	49.8	-1.87	0.0366	-4.97		0.485
	50.9	-1.88	0.0201	-5.35	0.304	0.536

Using equation (4.2) and TD as the response once again, R^2 values as seen in Table 4.8 were as follows: temperature difference at 1 P.M., 0.74; temperature gain from 6 A.M. to 1 P.M., 0.77; and peak soil temperature, 0.74.

Table 4.8 Revised 5-cm Multiple Linear Regression Coefficients for All Data

	Regression Coefficients					
		SR	WSWC	WS	RH	
	a_0	a_1	a_2	a_3	a_4	R^2
Difference	0.7	0.0201				0.392
	8.8	0.0196	-0.287			0.651
	15.3	0.0203	-0.303	-2.19		0.729
	10.1	0.0221	-0.324	-2.09	0.0734	0.740
Gain	1.6	0.0230				0.439
	10.2	0.0224	-0.302			0.686
	17.5	0.0233	-0.320	-2.47		0.771
	19.7	0.0225	-0.312	-2.51	-0.0302	0.772
Peak	0.6	0.0234				0.316
Soil Temp	7.5	0.0234	-0.255			0.607
	17.8	0.0219	-0.278	-2.63		0.740
	18.7	0.0218	-0.272	-2.64	-0.0183	0.741

Using equation (4.2) R^2 values as seen in Table 4.9 were as follows: temperature difference at 1 P.M., 0.71; temperature gain from 6 A.M. to 1 P.M., 0.70; and peak soil temperature, 0.67.

Table 4.9 Revised 5-cm Multiple Linear Regression Coefficients for Select Data

	Regression Coefficients					
		SR	WSWC	WS	RH	
	a_0	a_1	a_2	a_3	a_4	R^2
Difference	9.19	0.0110				0.042
	6.89	0.0242	-0.372			0.517
	19.31	0.0187	-0.358	-2.51		0.667
	14.24	0.0175	-0.379	-2.46	0.124	0.706
Gain	13.26	0.0104				0.035
	10.86	0.0240	-0.387			0.519
	25.10	0.0177	-0.370	-2.88		0.704
	24.52	0.0176	-0.372	-2.87	0.014	0.705
Peak	2.25	0.0224				0.180
Soil Temp	7.87	0.0233	-0.260			0.489
	20.71	0.0186	-0.260	-2.66		0.670
	21.28	0.0138	-0.274	-2.76	0.087	0.668

In the 10-cm soil depth multiple linear regressions, it must be noted that relative humidity had the highest correlation strength in determining weighted soil water content. However, in the 5-cm soil depth the correlation strength of relative humidity dropped off and was only the third most important variable. The likely cause is from April 27th to June 30th only rainfall was necessary to increase weighted soil water content while from August to September 5th additional water was manually added due to lack of rainfall. This accounts for roughly half the time testing was being performed on the 5-cm soil depth. The strong correlation was a result of high humidity conditions taking place shortly after rainfall, or when weighted soil water content is high, while low relative humidity conditions took place many days after a rainfall event when weighted soil water content was much lower.

4.3 Feedlot Surface

Of the seven days tested on a feedlot surface, only four days were useable to the calibrated equations. The fifth day experienced rainfall while day six and seven experienced standing water on the soil surface. Table 4.10 shows meteorological variables used for the single measurement at 1 P.M. method as well as temperature change from 6 A.M. to 1 P.M. Table 4.11 shows conditions used to estimate soil water at peak temperature of the soil surface.

Table 4.10 Meteorological Variables at Feedlot

					Air Temp		Soil Temp		Difference	Change
	WSWC	WS	RH	SR	6:00 AM	1:00 PM	6:00 AM	1:00 PM	1:00 PM	6 AM to 1 PM
9/19/2010	4.2	0.8	69.6	776	10.2	18.8	15.2	51.7	32.9	27.9
9/20/2010	4.1	11.0	32.9	768	20.3	29.6	19.5	43.1	13.5	14.3
9/21/2010	9.1	6.3	50.2	762	21.4	28.8	20.9	42.0	13.2	13.7
9/22/2010	6.0	9.3	50.3	841	20.1	29.3	20.1	42.5	13.2	13.2

Table 4.11 Meteorological Variables at Feedlot during Peak Soil Surface Temperature

	WSWC	WS	RH	SR	Air Temp	Soil Temp	Time
9/19/2010	4.2	3.0	42.3	728	27.6	54.8	2:55 PM
9/20/2010	4.1	11.1	31.0	787	29.6	43.9	1:30 PM
9/21/2010	9.1	6.3	50.2	924	28.8	47.2	12:45 PM
9/22/2010	6.0	9.0	44.6	1003	30.1	44.6	2:00 PM

Conditions were extreme at the time of testing due to no precipitation events at the site since August 23rd resulting in very dry soil surface. Wind gusts were also very high causing dust events in the feedlot. This caused the wind component of the equation to go out of the range in which the regressions were performed. The highest wind speed measured was 5.2 m/s for the 5-cm soil depth on the Agronomy Research Farm, while 11.1 m/s wind speeds were measured near the feedlot. This caused the soil surface to peak at 43.9°C with 11.1 m/s winds compared to 54.8°C with only 3.0 m/s wind speeds on similar days with equal surface water content.

Table 4.12 estimates surface soil water using the multiple linear regression equation from the 5-cm soil depth. All three methods were used and compared. The equations did not perform with high accuracy, but were able to differentiate the four different surface soil water conditions that differed from 4.1% to 9.1% on a wet basis.

Table 4.12 Estimate Surface Soil Water Using 5-cm Soil Depth Equation

	Actual	Temperature Gain	1:00 PM Difference	Peak Difference
9/19/2010	4.2	25.3	12.7	8.5
9/20/2010	4.1	-3.6	-5.7	-13.0
9/21/2010	9.1	20.5	16.7	15.6
9/22/2010	6.0	11.3	9.4	10.0

CHAPTER 5 - Conclusions and Recommendations

5.1 Conclusions

The thermal inertia approach was selected as the remote sensing technique to apply for this application due to its low cost, ground level approach, and inherent ability to measure surface water before the evening dust peak that is associated with large cattle feedlots.

Controlled laboratory testing performed the best at predicting soil water content with the highest R^2 values at 0.91 with the Smolan silt loam. No significant increase in R^2 values was observed with an increase in the heating/cooling time, indicating that the method can measure soil water relatively quickly. Possible error in testing could have manifested in voltage drops that will fluctuate the light intensity of the lamp. With the Smolan silt loam a soil water probe was used due to its ability to continuously monitor water status in the soil. This allowed for the soil to remain undisturbed, with no need to collect samples for oven drying. As a result, the soil water content measured was integrated over the length of the 45-mm metal rods. The dried feedlot soil could not support the probe, thus oven drying was necessary to measure soil water. Oven drying meant the measured water content was closer to the surface. Highest R^2 values for the dried feedlot soil were 0.83.

Outdoor testing on the 10-cm soil layer did not achieve desirable results using equation (2.12) with R^2 values only as high as 0.38 for both the general data set and select data in terms of multiple linear regressions. The 5-cm soil layer performed better with R^2 values of 0.59 for the general data set and 0.67 for select data. Using equation (4.2) R^2 values increased notably for the 10-cm soil depth with a maximum R^2 value of 0.81 using the temperature gain from 6 A.M. to 1 P.M. method. The 5-cm soil depth also saw increased model strength with the highest R^2 value of 0.77 using the same method.

Feedlot testing proved to be imprecise, but was able to differentiate surface soil water conditions varying from 4.1% to 9.1% wet basis. In order for precise measurements of surface soil water, more extensive modeling of meteorological variables along with knowledge of soil properties would have to be done.

Calibrating an equation to predict surface soil water based on the method that was performed has downfalls. Performing regressions on selected data can pick up on relationships in the data that may have no direct physical relationship with each other. This shows when performing regressions, precaution must be taken in understanding the true mechanisms causing an event. Correlation does not equal causation. This is the case when using wind speed and relative humidity as predictors of soil water. Varying wind speed or relative humidity has no direct link to differences in soil water, but do influence the temperature difference between the soil surface and air to an extent. The proper physical relationship is TD = *f*(WSWC, SR, WS, RH). All four regressors then truly help predict the soil surface and air temperature difference. The problem lies in that WSWC is unknown while TD, SR, WS, and RH are known using this methodology.

The best way to estimate surface soil water would be to model each meteorological variable independently to show the proper relationship to the temperature difference between the soil surface and air temperature. Soil water, wind speed, and relative humidity were found to be all negatively correlated with soil surface to air temperature difference, meaning as each variable increases, soil surface to air temperature difference decreases. Solar radiation was positively correlated. Possibly the largest increase in accuracy would be proper modeling of incoming solar radiation since it can fluctuate significantly throughout the day depending on cloud cover. Large fluctuations were seen in the soil surface to air temperature difference in short time intervals when solar radiation could increase from low to high values and vice versa.

5.2 Recommendations for Future Research

The soil thermal inertia approach cannot provide an instantaneous soil water measurement such as RADAR. It requires multiple weather parameters to be collected and calibrated to fit to unique soil characterizations. Proper heat transfer properties of the soil are also needed to provide accurate measurement. With high R^2 values in some cases, the method has promise. A long-term data set would be necessary to produce enough days and conditions for the models. More advanced models (e.g., non-linear) might be needed to accurately characterize the energy balance and increase the effectiveness of the method. It is also necessary to statistically analyze the data more fully (e.g., statistical significance of the regression models and multicolinearity of the predictors).

CHAPTER 6 - References

Alshikaili, T.Y. 2007. Non-contact measurement of soil moisture content using thermal infrared sensor and weather variables. MS thesis. Saskatoon, Saskatchewan: University of Saskatchewan, Department of Agricultural and Bioresource Engineering.

Auvermann, B. 2001. Controlling dust and odor from open lot livestock facilities. Lesson 42, Livestock and Poultry Environmental Stewardship Curriculum: A National Educational Program. Ames, IA: Midwest Plan Service.

Bolander, P. and A. Yamada. 1999. Dust palliative selection and application guide. Washington, DC: United States Department of Agriculture, Forest Service.

Bonifacio, H.F. 2009. Particulate matter emissions from commercial beef cattle feedlots in Kansas. MS thesis. Manhattan, Kansas: Kansas State University, Department of Biological and Agricultural Engineering.

Bowers, S.A. and R.J. Hanks. 1965. Reflection of radiant energy from soils. *Soil Science* 100(2):130-138.

Campbell Scientific, Inc. 2010. Logan, UT. Available at: http://www.campbellsci.com. Accessed 12 April 2010

Cole, N.A., R. Todd, B. Auvermann, and D. Parker. 2008. Auditing and assessing air quality in concentrated feeding operations. *The Professional Animal Scientist* 24:1-22.

Control Company. 2010. Friendswood, TX Available at: http://www.control3.com/. Accessed 27 August 2010.

Datt, B. 1999. Remote sensing of water content in *Eucalyptus* leaves. *Australian Journal of Botany* 47:909-923.

EPA. 2009. Animal Feeding Operations. Washington, D.C.: Environmental Protection Agency. Available at: http://www.epa.gov/oecaagct/anafoidx.html. Accessed 16 February 2009.

EPA. 2010. National Ambient Air Quality Standards (NAAQS). Washington, D.C.: Environmental Protection Agency. Available at http://www.epa.gov/air/criteria.html. Accessed 12 August 2010.

Everitt, J.H., D.E. Escobar, M.A. Alaniz, and M.R. Davis. 1989. Using multispectral video imagery for detecting soil surface conditions. *Photogrammetric Engineering and Remote Sensing* 55(4):467-471.

Fernandez-Galvez, J. 2008. Errors in soil moisture content estimates induced by uncertainties in the effective soil dielectric constant. *International Journal of Remote Sensing* 29(10):3317-3323.

Hain, C.R., J.R. Mecikalski, and M.C. Anderson. 2009. Retrieval of an available water-based soil moisture proxy from thermal infrared remote sensing. Part I: Methodology and validation. *Journal of Hydrometeorology* 10(3):665-683.

Hulley, G.C., S.J. Hook, and A.M. Baldridge. 2010. Investigating the effects of soil moisture on thermal infrared land surface temperature and emissivity using satellite retrievals and laboratory measurements. *Remote Sensing of Environment* 114:1480-1493.

ICT International. 2010. Armidale, Australia. Available at: www.ictinternational.com.au. Accessed 9 August 2010.

Irrometer. 2010. Riverside, CA. Available at www.irrometer.com. Accessed 9 August 2010.

Jensen, J.R. 2007. *Remote Sensing of the Environment: An Earth Resource Perspective*. 2nd ed. Upper Saddle River, NJ.: Pearson Prentice Hall.

Kano, Y., W.F. McClure, and R.W. Skaggs. 1985. A near infrared reflectance soil moisture meter. *Transactions of the ASAE* (28)6:1852-1855.

Kelly, R., T. Davie, and P. Atkinson. 2003. Explaining temporal and spatial variation in soil moisture in a bare field using SAR imagery. *International Journal of Remote Sensing* 24(15):3059-3074.

Ledieu, J., P. De Ridder, P. De Clerck, and S. Dautrebande. 1986. A method of measuring soil moisture by time-domain reflectometry. *Journal of Hydrology* 88:319-328.

Marek, G., T. Marek, K. Heflin, and B. Auvermann. 2004. Determination of feedyard evaporation using weighing lysimeters. ASAE Paper No. 044014. St. Joseph, MI: ASAE.

McCumber, M.C. and R.A. Pielke. 1981. Simulation of the effects of surface fluxes of heat and moisture in a mesoscale numerical-model .1. soil layer. *Journal of Geophysical Research* 86: 9929-9938.

Minacapilli, M., M. Iovino, and F. Blanda. 2009. High resolution remote estimation of soil surface water content by a thermal inertia approach. *Journal of Hydrology* 379(3-4):229-238.

Mira, M., E. Valor, R. Boluda, V. Caselles, and C. Coll. 2007. Influence of soil water content on the thermal infrared emissivity of bare soil: Implication for land surface temperature determination. *Journal of Geophysical Research* 112(f4):1-11.

Mira, M, E. Valor, V. Caselles, E. Rubio, C. Coll, J.M. Galve, R. Niclos, J.M. Sanchez, and R. Boluda. 2010. Soil moisture effect on thermal infrared (8-13-µm) emissivity. *IEEE Transactions on Geoscience and Remote Sensing* 48(5):2251-2260.

Moore, D.G., M.L. Horton, J.J. Russell, and V.I. Myers. 1975. Evaluation of Thermal X/5 Detector Skylab S-192 Data for Estimating Evapotranspiration and Thermal Properties of Soils for Irrigation Management. Proc. of the NASA Earth Resources Survery Symp., Houston, Texas, NASA TX X-58168, p2561-2583.

Myhre, B.E. and S.F. Shih. 1990. Using infrared thermometry to estimate soil water content for a sandy soil. *Transactions of the ASAE* 33(5):1479-1486.

NRC. National Research Council (U.S.), Ad Hoc, and Board on National Research Council (U.S.). 2003. *Air Emissions from Animal Feeding Operations: Current Knowledge, Future Needs*. New York: National Academies Press.

Shih, S.F. and J.D. Jordan. 1992. Landsat mid-infrared data and GIS in regional surface soil-moisture assessment. *Water Resources Bulletin* 28(4):713-719.

Soilmoisture Equipment Corp. 2010. Santa Barbara, CA. Available at: www.soilmoisture.com. Accessed 9 August 12 2010.

Stevens Water Monitoring Systems, Inc. 2010. Portland, OR. Available at http://www.stevenswater.com. Accessed 12 April, 2010.

Sweeten, J.M. and S. Lott. 1994. Dust Management. In P.J. Watts and R. Tucker, eds., Designing Better Feedyards. Toowoomba, Queensland: Queensland Department of Primary Industries.

Sugiura, R., N. Noguchi, and K. Ishii. 2007. Correction of low-altitude thermal images applied to estimating soil water status. *Biosystems Engineering* 96(3):301-313.

Transducer Techniques. 2010. Temecula, CA. Available at: http://www.transducertechniques.com. Accessed 12 April 2010.

USDA. 2010. Animal Production. Washington, D.C.: United States Department of Agriculture. Available at: http://www.usda.gov. Accessed 24 August 2010.

Ward, A.D. and S.W. Trimble. 2004. *Environmental Hydrology*. 2nd ed. Boca Raton, Florida.: Lewis Publishers.

Waring, R.H., J. Way, E.R. Hunt, L. Morrissey, K.J. Ranson, J.F. Weishampel, R. Oren, and S.E. Franklin. 1995. Imaging radar for ecosystem studies. *BioScience* 45(10):715-723.

Wheeler, P.A. and G.L. Duncan. 1984. Measuring soil moisture electromagnetically. *Agricultural Engineering* 69(9):12-15.

Appendix A - Supporting Information for Chapter 3

Power requirements:	none, self-powered	**Output:**	0.2 mV per W m^{-2}
Absolute accuracy:	±5% for daily total radiation	**Measurement range:**	0 to 2000 W m^{-2} (full sunlight ≈ 1000 W m^{-2})
Cosine response:	±4% at 75° zenith angle ±1% at 45° zenith angle	**Light spectrum waveband:**	300 to 1100 nm
Temperature response:	<1% at 5° to 40°C	**Dimensions**	
		Height:	1.0 inch (2.5 cm)
Long-term stability:	<2% per year	**Diameter:**	0.9 inch (2.4 cm)
Operating temperature:	-40° to +55°C	**Weight:**	2.3 oz (65 g) with 2 m cable length
Relative humidity:	0 to 100%		

Figure A.1 CS300 Apogee Silicon Pyranometer Specifications

Specifications

Ranges:	
Lux:	0 to 1999 Lux 2000 to 19,990 Lux 20,000 to 50,000 Lux
Foot Candle:	0 to 199.9 200 to 1999 2000 to 5000
Resolution:	1 Lux (0 to 1999 Lux) 10 Lux (2000 to 19,990 Lux) 100 Lux (20,000 to 50,000 Lux) 0.1 Foot Candle (0 to 199.9 Fc) 1 Foot Candle (200 to 1999 Fc) 10 Foot Candle (2000 to 5000 Fc)
Accuracy:	± 5% full scale plus 2 digits
Sampling Time:	Slow and Fast Response
Case:	ABS plastic
Fail safe:	Low battery indicator
Power:	One (1) 9-Volt alkaline battery
Accessories Supplied:	carrying case, photo sensor probe, battery, Traceable® Certificate, instructions.

Figure A.2 Control Company Traceable Dual-Range Light Meter Specifications

Datalogger Channels:
one differential (thermopile) and one single-ended (thermistor); please note that our CR200-series dataloggers are not compatible.

Input Power:
2.5 V excitation for thermistor

Absolute Accuracy:
±0.2°C @ -10° to +65°C; ±0.5°C @ -40° to +70°C

Uniformity:
±0.1°C @ -10° to +65°C; ±0.3°C @ -40° to +70°C

Repeatability:
±0.05°C @ -10° to +65°C; ±0.1°C @ -40° to +70°C

Response Time:
<1 s to changes in target temperature

Target Temperature Output Signal:
60 µV per °C difference from sensor body

Body Temperature Output Signal:
0 to 2500 mV

Optics:
Germanium lens

Wavelength Range:
8 to 14 µm (corresponds to atmospheric window)

Field of View (FOV):
22° half angle. The FOV is reported as the half-angle of the apex of the cone formed by the target (cone base) and the detector (cone apex). The target is a circle from which 98% of the radiation viewed by the detector is being emitted.

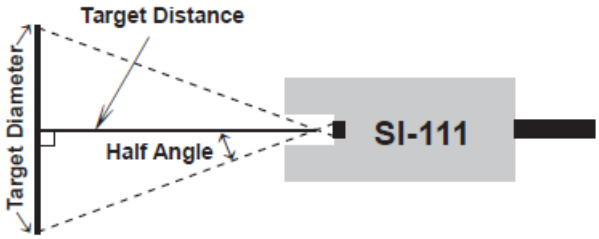

Operating Range: -55° to +80°C; 0 to 100% RH

Cable Description:
15' (4.5 m) twisted, shielded 4-conductor wire with Santoprene casing, ending in pigtails.

Dimensions:
0.9" (2.3 cm) diameter, 2.4" (6 cm) length

Weight:
6.7 oz. (190 g)

Figure A.3 SI-111 Precision Infrared Radiometer Specifications

Table A.1 SI-111 Precision Infrared Radiometer Wiring Program

Sensor/Lead	Description	CR10X	CR1000
SI-111 Thermopile	Target Temp		
Red	Diff. High	2H	2H
Black	Diff. Low	2L	2L
Clear	Analog Ground	AG	⏚
SI-111 Thermistor	Sensor Temp		
Green	SE	1	1
Blue	Analog Ground	AG	⏚
White	Excitation	E1	VX1 or EX1

Table A.2 Stevens Hydra Probe II Soil Water Sensor Technical Specifications

TECHNICAL SPECIFICATIONS		
Measurements	**Range**	**Accuracy**
Dielectric Constant	1 to 78 where 1 = air 78 = distilled water	± 1.5% or 0.2 whichever is typically greater
Soil Moisture for inorganic & mineral soil	From completely dry to fully saturated	± 0.03 water fraction by volume in typical soil
Conductivity	0.01 to 1.5 S/m	± 2.0% or 0.005 S/m whichever is typically greater
Temperature	-10° to +65° C	± 0.1° C

ELECTRICAL OPERATION		
	SDI-12	**RS485**
Electrical	9-20 VDC	9-20 VDC
Communication Protocol	SDI-12 Standard v. 1.2	Custom or open spec
Cable Length	60 meters/197 feet	1219 meters/4000 feet (max. non-spliced 304.8m /1000 ft)
Power	<1 mA idle 30 mA active	<10 mA idle 30 mA active
Cable	3-wire: power, ground, data	4-wire: power, ground, com+, com-
Baud Rate	1200	9600
Intersensor Variability	± 0.012 WFV (θ m^3 m^{-3})	± 0.012 WFV (θ m^3 m^{-3})

Electrical specifications are valid over a -25° to +50°C range unless otherwise specified; non-condensing environment required. To maintain electrical specifications, Campbell Scientific recommends recalibrating dataloggers every two years. We recommend that you confirm system configuration and critical specifications with Campbell Scientific before purchase.

PROGRAM EXECUTION RATE
10 ms to 30 min. @ 10 ms increments

ANALOG INPUTS
3 differential (DF) or 6 single-ended (SE) individually configured. Channel expansion provided by AM16/32B and AM25T multiplexers.

RANGES and RESOLUTION: Basic resolution (Basic Res) is the A/D resolution of a single conversion. Resolution of DF measurements with input reversal is half the Basic Res.

	Input Referred Noise Voltage	
Input Range (mV)[1]	DF Res (µV)[2]	Basic Res (µV)
±5000	667	1333
±2500	333	667
±250	33.3	66.7
±25	3.33	6.7
±7.5	1.0	2.0
±2.5	0.33	0.67

[1]Range overhead of ~9% exists on all ranges to guarantee that full-scale values will not cause over range.

[2]Resolution of DF measurements with input reversal.

ACCURACY[3]:
±(0.06% of reading + offset), 0° to 40°C
±(0.12% of reading + offset), -25° to 50°C
±(0.18% of reading + offset), -55° to 85°C (-XT only)

[3]The sensor and measurement noise are not included and the offsets are the following:
Offset for DF w/input reversal = 1.5·Basic Res + 1.0 µV
Offset for DF w/o input reversal = 3·Basic Res + 2.0 µV
Offset for SE = 3·Basic Res + 3.0 µV

INPUT NOISE VOLTAGE: For DF measurements with input reversal on ±2.5 mV input range; digital resolution dominates for higher ranges.
250 µs Integration: 0.34 µV RMS
50/60 Hz Integration: 0.19 µV RMS

MINIMUM TIME BETWEEN VOLTAGE MEASUREMENTS: Includes the measurement time and conversion to engineering units. For voltage measurements, the CR800-series integrates the input signal for 0.25 ms or a full 16.66 ms or 20 ms line cycle for 50/60 Hz noise rejection. DF measurements with input reversal incorporate two integrations with reversed input polarities to reduce thermal offset and common mode errors and therefore take twice as long.
250 µs Analog Integration: ~1 ms SE
1/60 Hz Analog Integration: ~20 ms SE
1/50 Hz Analog Integration: ~25 ms SE

INPUT LIMITS: ±5 V

DC COMMON MODE REJECTION: >100 dB

NORMAL MODE REJECTION: 70 dB @ 60 Hz when using 60 Hz rejection

SUSTAINED INPUT VOLTAGE W/O DAMAGE: ±16 Vdc max.

INPUT CURRENT: ±1 nA typical, ±6 nA max. @ 50°C; ±90 nA @ 85°C

INPUT RESISTANCE: 20 Gohms typical

ACCURACY OF BUILT-IN REFERENCE JUNCTION THERMISTOR (for thermocouple measurements):
±0.3°C, -25° to 50°C
±0.8°C, -55° to 85°C (-XT only)

ANALOG OUTPUTS
2 switched voltage, active only during measurement, one at a time.

RANGE AND RESOLUTION: Voltage outputs programmable between ±2.5 V with 0.67 mV resolution.

ACCURACY: ±(0.06% of setting + 0.8 mV), 0° to 40°C
±(0.12% of setting + 0.8 mV), -25° to 50°C
±(0.18% of setting + 0.8 mV), -55° to 85°C (-XT only)

CURRENT SOURCING/SINKING: ±25 mA

RESISTANCE MEASUREMENTS
MEASUREMENT TYPES: The CR800-series provides ratiometric measurements of 4- and 6-wire full bridges, and 2-, 3-, and 4-wire half bridges. Precise, dual polarity excitation using any of the 3 switched voltage excitations eliminates dc errors.

RATIO ACCURACY[4]: Assuming excitation voltage of at least 1000 mV, not including bridge resistor error.
±(0.04% of voltage reading + offset)/V_x

[4]The sensor and measurement noise are not included and the offsets are the following:
Offset for DF w/input reversal = 1.5·Basic Res + 1.0 µV
Offset for DF w/o input reversal = 3·Basic Res + 2.0 µV
Offset for SE = 3·Basic Res + 3.0 µV
Offset values are reduced by a factor of 2 when excitation reversal is used.

PERIOD AVERAGING MEASUREMENTS
The average period for a single cycle is determined by measuring the average duration of a specified number of cycles. The period resolution is 192 ns divided by the specified number of cycles to be measured; the period accuracy is ±(0.01% of reading + resolution). Any of the 6 SE analog inputs can be used for period averaging. Signal limiting are typically required for the SE analog channel.

INPUT FREQUENCY RANGE:

Input Range	Signal (peak to peak)[5] Min	Max	Min. Pulse W.	Max[6] Freq.
±2500 mV	500 mV	10 V	2.5 µs	200 kHz
±250 mV	10 mV	2 V	10 µs	50 kHz
±25 mV	5 mV	2 V	62 µs	8 kHz
±2.5 mV	2 mV	2 V	100 µs	5 kHz

[5]The signal is centered at the datalogger ground.

[6]The maximum frequency = 1/(Twice Minimum Pulse Width) for 50% of duty cycle signals.

PULSE COUNTERS
Two 24-bit inputs selectable for switch closure, high frequency pulse, or low-level ac.

MAXIMUM COUNTS PER SCAN: 16.7 x 10^6

SWITCH CLOSURE MODE:
Minimum Switch Closed Time: 5 ms
Minimum Switch Open Time: 6 ms
Max. Bounce Time: 1 ms open w/o being counted

HIGH FREQUENCY PULSE MODE:
Maximum Input Frequency: 250 kHz
Maximum Input Voltage: ±20 V
Voltage Thresholds: Count upon transition from below 0.9 V to above 2.2 V after input filter with 1.2 µs time constant.

LOW LEVEL AC MODE: Internal ac coupling removes dc offsets up to ±0.5 V.
Input Hysteresis: 12 mV @ 1 Hz
Maximum ac Input Voltage: ±20 V
Minimum ac Input Voltage:

Sine wave (mV RMS)	Range (Hz)
20	1.0 to 20
200	0.5 to 200
2000	0.3 to 10,000
5000	0.3 to 20,000

DIGITAL I/O PORTS
4 ports software selectable, as binary inputs or control outputs. They also provide edge timing, subroutine interrupts/wake up, switch closure pulse counting, high frequency pulse counting, asynchronous communications (UART), SDI-12 communications, and SDM communications.

HIGH FREQUENCY MAX: 400 kHz

SWITCH CLOSURE FREQUENCY MAX: 150 Hz

OUTPUT VOLTAGES (no load): high 5.0 V ±0.1 V; low <0.1

OUTPUT RESISTANCE: 330 ohms

INPUT STATE: high 3.8 to 16 V; low -8.0 to 1.2 V

INPUT HYSTERISIS: 1.4 V

INPUT RESISTANCE: 100 kohms

SERIAL DEVICE/RS-232 SUPPORT: 0 to 5 V UART

SWITCHED 12 V
One independent 12 V unregulated source is switched on and off under program control. Thermal fuse hold current = 900 mA @ 20°C, 650 mA @ 50°C, 360 mA @ 85°C.

SDI-12 INTERFACE SUPPORT
Control ports 1 and 3 may be configured for SDI-12 asynchronous communications. Up to ten SDI-12 sensors are supported per port. It meets SDI-12 Standard version 1.3 for datalogger mode.

CE COMPLIANCE
STANDARD(S) TO WHICH CONFORMITY IS DECLARED: IEC61326:2002

CPU AND INTERFACE
PROCESSOR: Renesas H8S 2322 (16-bit CPU with 32-bit internal core)

MEMORY: 2 MB of Flash for operating system; 4 MB of battery-backed SRAM for CPU usage, program storage and data storage

CLOCK ACCURACY: ±3 min. per year

PROTOCOLS SUPPORTED: PakBus, Modbus, DNP3, FTP, HTTP, XML, POP3, SMTP, Telnet, NTCIP, NTP, SDI-12, SDM

SERIAL INTERFACES: CS I/O port is used to interface with Campbell Scientific peripherals; RS-232 DCE port is for computer or non-CSI modem connection. Baud rates are selectable from 300 bps to 115.2 kbps. ASCII protocol is one start bit, one stop bit, eight data bits, and no parity.

SYSTEM POWER REQUIREMENTS
VOLTAGE: 9.6 to 16 Vdc

TYPICAL CURRENT DRAIN:
Sleep Mode: ~0.6 mA
1 Hz Scan (60 Hz rejection)
w/RS-232 communication: 19 mA
w/o RS-232 communication: 4.2 mA
1 Hz Scan (250 µs integration)
w/RS-232 communication: 16.7 mA
w/o RS-232 communication: 1 mA
100 Hz Scan (250 µs integration)
w/RS-232 communication: 27.6 mA
w/o RS-232 communication: 16.2 mA

CR1000KD OR CR850'S ON-BOARD KEYBOARD DISPLAY CURRENT DRAIN:
Inactive: negligible
Active w/o backlight: 7 mA
Active w/backlight: 100 mA

EXTERNAL BATTERIES: 12 Vdc nominal; reverse polarity protected.

PHYSICAL SPECIFICATIONS
DIMENSIONS: 9.5" x 4.1" x 2" (24.1 x 10.4 x 5.1 cm); additional clearance required for serial cable and sensor leads.

WEIGHT: 1.5 lbs (0.7 kg)

WARRANTY
3 years against defects in materials and workmanship.

Figure A.4 CR800 Datalogger Specifications

8 differential (16 single-ended) analog input channels
4 switched excitation outputs
2 continuous analog outputs
6 control ports
4 pulse counting channels
Stored 19,296 data points in internal memory

Figure A.5 21X Specifications

Rated Output (R.O.):2 mV/V nominal
Nonlinearity:0.1% of R.O.
Hysteresis:0.1% of R.O
Nonrepeatability:0.05% of R.O.
Zero Balance:1.0% of R.O.
Compensated Temp. Range:60° to 160°F
Safe Temp. Range:-65° to 200°F
Temp. Effect on Output:0.005% of Load/°F
Temp. Effect on Zero:0.005% of R.O./°F
Terminal Resistance:350 ohms nominal
Excitation Voltage:10 VDC
Safe Overload:150% of R.O.
Calibration Included:Compression
Optional Calibration:Tension

Figure A.6 Load Cell Specifications

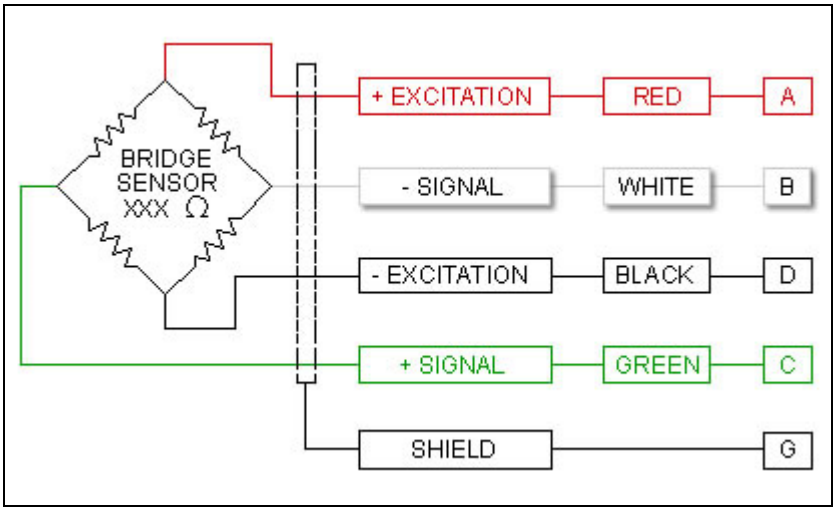

Figure A.7 Load Cell Wiring Diagram

Appendix B - Supporting Information for Chapter 4

Table B.1 Meteorological Variables for 5-cm Soil Depth Select Data

	SM	WS	RH	SR	TempDiff
7/2/2010	49.4	3.88	55.2	939	10.4
7/9/2010	44.0	2.35	56.3	893	19.0
7/11/2010	38.1	3.86	48.7	1145	20.9
7/13/2010	33.6	3.34	69.8	982	19.7
7/14/2010	30.1	4.24	63.0	920	18.3
7/15/2010	50.8	2.62	70.1	910	8.7
7/16/2010	43.2	1.70	61.8	886	15.6
7/17/2010	37.8	2.50	64.7	917	22.2
7/18/2010	32.8	2.81	60.1	985	18.9
7/22/2010	34.6	4.88	54.8	906	15.2
7/23/2010	29.1	4.97	55.0	823	17.0
7/24/2010	25.1	2.44	57.8	910	23.1
7/25/2010	22.9	2.40	63.6	950	26.7
7/26/2010	20.7	2.02	56.3	965	27.2
7/27/2010	17.4	2.39	56.2	895	26.0
7/28/2010	14.2	2.57	53.5	891	27.3
7/29/2010	11.3	2.05	54.6	1006	30.0
7/30/2010	8.7	3.69	53.6	401	14.5
7/31/2010	19.8	2.00	60.7	1015	20.0
8/1/2010	12.3	2.78	53.2	963	26.2
8/2/2010	8.9	2.96	43.9	894	22.7
8/3/2010	36.2	2.62	45.3	889	7.3
8/4/2010	26.5	4.39	61.1	605	13.8
8/5/2010	22.8	3.17	50.3	913	24.8
8/6/2010	18.0	2.43	51.6	929	23.9
8/7/2010	14.4	2.75	55.9	945	26.9
8/8/2010	11.0	2.94	48.7	858	24.5
8/9/2010	6.9	2.99	44.0	836	23.4
8/11/2010	31.7	1.65	51.8	864	18.7
8/12/2010	24.2	3.03	45.8	859	21.0
8/19/2010	38.5	3.29	50.6	883	7.7
8/21/2010	27.2	2.78	59.8	896	20.8
8/22/2010	21.6	3.14	51.6	843	20.2
8/23/2010	17.0	3.27	55.2	834	19.3
8/24/2010	43.2	4.36	56.9	1044	5.3
8/25/2010	32.3	2.76	29.3	846	14.7
8/26/2010	25.9	1.87	33.5	843	17.9
8/27/2010	21.3	2.99	31.1	842	19.5
8/28/2010	16.8	3.54	33.5	840	15.2
8/29/2010	12.4	4.74	49.5	855	16.3
8/30/2010	8.8	3.85	56.5	714	19.1
8/31/2010	5.8	4.61	55.4	826	17.9
9/3/2010	31.6	5.18	37.7	865	5.5
9/4/2010	25.2	2.28	31.6	828	20.0
9/5/2010	20.1	4.87	37.4	818	17.1

```
proc reg data=work.twoa;
      model sm=tempdiff sr ws rh/clb clm cli ss1 influence vif;
print;
run;
```

The SAS System

The REG Procedure
Model: MODEL1
Dependent Variable: SM SM

Number of Observations Read	45
Number of Observations Used	45

Analysis of Variance

Source	DF	Sum of Squares	Mean Square	F Value	Pr > F
Model	4	4115.30279	1028.82570	20.67	<.0001
Error	40	1990.78299	49.76957		
Corrected Total	44	6106.08578			

Root MSE	7.05476	R-Square	0.6740
Dependent Mean	24.98222	Adj R-Sq	0.6414
Coeff Var	28.23910		

Parameter Estimates

Variable	Label	DF	Parameter Estimate	Standard Error	t Value	Pr > |t|	Type I SS	Variance Inflation
Intercept	Intercept	1	15.95161	11.84959	1.35	0.1858	28085	0
TempDiff	TempDiff	1	-1.62629	0.20273	-8.02	<.0001	2061.98098	1.30565
SR	SR	1	0.04137	0.01000	4.14	0.0002	1313.19850	1.09950
WS	WS	1	-3.65460	1.28243	-2.85	0.0069	398.18090	1.31525
RH	RH	1	0.28545	0.10890	2.62	0.0123	341.94241	1.04093

Parameter Estimates

Variable	Label	DF	95% Confidence Limits	
Intercept	Intercept	1	-7.99730	39.90053
TempDiff	TempDiff	1	-2.03603	-1.21655
SR	SR	1	0.02116	0.06157
WS	WS	1	-6.24648	-1.06272
RH	RH	1	0.06535	0.50555

The SAS System

The REG Procedure
Model: MODEL1
Dependent Variable: SM SM

Output Statistics

Obs	Dependent Variable	Predicted Value	Std Error Mean Predict	95% CL Mean		95% CL Predict		Residual
1	49.4000	39.4583	2.0884	35.2374	43.6792	24.5885	54.3282	9.9417
2	44.0000	29.4749	1.5304	26.3817	32.5680	14.8850	44.0647	14.5251
3	38.1000	29.1214	3.2161	22.6213	35.6214	13.4515	44.7913	8.9786
4	33.6000	32.2536	2.3181	27.5686	36.9386	17.2454	47.2618	1.3464
5	30.1000	26.7355	2.1290	22.4325	31.0384	11.8422	41.6288	3.3645
6	50.8000	49.8814	3.4078	42.9940	56.7688	34.0469	65.7159	0.9186
7	43.2000	38.6602	2.7198	33.1633	44.1570	23.3791	53.9412	4.5398
8	37.8000	27.1131	1.8435	23.3872	30.8390	12.3761	41.8501	10.6869
9	32.8000	32.8468	1.6509	29.5102	36.1834	18.2034	47.4902	-0.0468
10	34.6000	26.5182	2.3370	21.7949	31.2415	11.4981	41.5384	8.0818
11	29.1000	19.8857	2.4359	14.9625	24.8088	4.8015	34.9699	9.2143
12	25.1000	23.6096	1.4863	20.6057	26.6134	9.0384	38.1807	1.4904
13	22.9000	21.2114	2.0706	17.0265	25.3963	6.3517	36.0710	1.6886
14	20.7000	20.3237	1.9795	16.3230	24.3244	5.5148	35.1325	0.3763
15	17.4000	17.9988	1.7126	14.5376	21.4601	3.3265	32.6711	-0.5988
16	14.2000	14.2906	1.8380	10.5759	18.0053	-0.4435	29.0248	-0.0906
17	11.3000	16.8712	2.3838	12.0533	21.6890	1.8210	31.9213	-5.5712
18	8.7000	10.7730	4.8346	1.0020	20.5440	-6.5119	28.0579	-2.0730
19	19.8000	35.4304	2.1548	31.0754	39.7853	20.5219	50.3388	-15.6304
20	12.3000	18.2048	1.7770	14.6134	21.7963	3.5013	32.9084	-5.9048
21	8.9000	17.7301	1.5745	14.5478	20.9123	3.1211	32.3391	-8.8301
22	36.2000	44.2103	2.9705	38.2066	50.2140	28.7397	59.6810	-8.0103
23	26.5000	19.9328	3.3110	13.2410	26.6247	4.1824	35.6833	6.5672
24	22.8000	16.1602	1.6338	12.8583	19.4622	1.5247	30.7958	6.6398
25	18.0000	21.3612	1.4728	18.3846	24.3379	6.7957	35.9268	-3.3612
26	14.4000	17.2022	1.8321	13.4993	20.9050	2.4710	31.9333	-2.8022
27	11.0000	14.7568	1.5748	11.5740	17.9396	0.1477	29.3659	-3.7568
28	6.9000	14.1113	1.6936	10.6883	17.5343	-0.5520	28.7746	-7.2113
29	31.7000	30.0368	2.2436	25.5023	34.5713	15.0749	44.9987	1.6632
30	24.2000	19.3335	1.3315	16.6423	22.0246	4.8235	33.8434	4.8665
31	38.5000	42.3759	2.4332	37.4583	47.2935	27.2935	57.4583	-3.8759
32	27.2000	26.0992	1.4000	23.2696	28.9288	11.5630	40.6355	1.1008
33	21.6000	21.2262	1.1579	18.8861	23.5664	6.7773	35.6752	0.3738
34	17.0000	22.8701	1.2380	20.3680	25.3723	8.3941	37.3462	-5.8701
35	43.2000	50.8269	3.4422	43.8700	57.7839	34.9621	66.6918	-7.6269
36	32.3000	25.3182	2.8361	19.5862	31.0501	9.9510	40.6854	6.9818
37	25.9000	24.4414	2.8553	18.6706	30.2122	9.0597	39.8231	1.4586
38	21.3000	17.0197	2.4953	11.9765	22.0629	1.8959	32.1436	4.2803
39	16.8000	22.6051	2.2758	18.0056	27.2046	7.6234	37.5868	-5.8051
40	12.4000	21.6184	2.1164	17.3409	25.8958	6.7324	36.5044	-9.2184
41	8.8000	16.4828	2.1885	12.0598	20.9059	1.5543	31.4113	-7.6828
42	5.8000	19.9759	2.1136	15.7042	24.2477	5.0916	34.8603	-14.1759
43	31.6000	34.6197	3.2471	28.0571	41.1822	18.9237	50.3156	-3.0197
44	25.2000	18.3649	2.6920	12.9243	23.8056	3.1040	33.6259	6.8351

The SAS System

The REG Procedure
Model: MODEL1
Dependent Variable: SM SM

Output Statistics

		Hat Diag	Cov		DFBETAS				
Obs	RStudent	H	Ratio	DFFITS	Intercept	TempDiff	SR	WS	RH
1	1.4981	0.0876	0.9404	0.4643	-0.0769	-0.3100	0.1847	0.0571	0.0860
2	2.2091	0.0471	0.6605	0.4909	0.1498	-0.1548	-0.0409	-0.3234	0.1488
3	1.4495	0.2078	1.1021	0.7424	-0.5297	0.1332	0.6449	0.3469	-0.1884
4	0.1996	0.1080	1.2658	0.0695	-0.0432	0.0007	0.0213	0.0136	0.0530
5	0.4955	0.0911	1.2101	0.1568	-0.0999	0.0269	0.0310	0.1024	0.0841
6	0.1469	0.2333	1.4763	0.0810	0.0098	-0.0606	0.0013	-0.0373	0.0498
7	0.6929	0.1486	1.2540	0.2895	0.1137	-0.1681	-0.0382	-0.2302	0.1206
8	1.5997	0.0683	0.8865	0.4331	-0.0827	0.0372	-0.0160	-0.1172	0.3028
9	-0.0067	0.0548	1.2007	-0.0016	0.0006	0.0004	-0.0008	0.0003	-0.0007
10	1.2216	0.1097	1.0566	0.4289	-0.2251	0.0332	0.1130	0.3519	0.0572
11	1.4087	0.1192	1.0054	0.5183	-0.1839	0.1437	-0.0499	0.4390	0.0934
12	0.2135	0.0444	1.1807	0.0460	-0.0024	0.0115	-0.0014	-0.0155	0.0166
13	0.2474	0.0861	1.2322	0.0760	-0.0292	0.0364	0.0063	-0.0063	0.0384
14	0.0549	0.0787	1.2315	0.0160	-0.0031	0.0075	0.0029	-0.0047	0.0018
15	-0.0864	0.0589	1.2049	-0.0216	0.0012	-0.0121	0.0030	0.0041	-0.0043
16	-0.0131	0.0679	1.2176	-0.0035	0.0004	-0.0026	0.0004	-0.0000	-0.0001
17	-0.8359	0.1142	1.1724	-0.3001	0.1052	-0.1866	-0.0950	0.0287	0.0089
18	-0.3992	0.4696	2.0967	-0.3757	-0.2532	0.0105	0.3604	0.0363	-0.0793
19	-2.4708	0.0933	0.6049	-0.7925	0.1240	0.2328	-0.3398	0.4336	-0.2700
20	-0.8621	0.0634	1.1027	-0.2244	0.0969	-0.1488	-0.0722	-0.0381	0.0129
21	-1.2949	0.0498	0.9678	-0.2965	-0.0308	-0.1347	-0.0285	-0.0222	0.1792
22	-1.2610	0.1773	1.1297	-0.5854	-0.3054	0.5136	-0.0613	0.3364	0.1083
23	1.0557	0.2203	1.2643	0.5611	0.1864	-0.0239	-0.4365	0.1158	0.2561
24	0.9667	0.0536	1.0654	0.2301	-0.0724	0.1674	0.0324	0.0845	-0.0451
25	-0.4825	0.0436	1.1519	-0.1030	0.0026	-0.0392	-0.0164	0.0284	0.0128
26	-0.4070	0.0674	1.1915	-0.1095	0.0459	-0.0776	-0.0194	-0.0176	-0.0126
27	-0.5415	0.0498	1.1506	-0.1240	-0.0095	-0.0838	0.0262	-0.0152	0.0314
28	-1.0545	0.0576	1.0464	-0.2608	-0.0746	-0.1431	0.0674	-0.0196	0.1321
29	0.2457	0.1011	1.2529	0.0824	0.0510	-0.0321	-0.0174	-0.0725	0.0012
30	0.6979	0.0356	1.1061	0.1341	0.0412	0.0432	-0.0186	-0.0001	-0.0668
31	-0.5804	0.1190	1.2340	-0.2133	-0.0752	0.1914	-0.0250	0.0724	-0.0021
32	0.1572	0.0394	1.1777	0.0318	-0.0032	0.0021	-0.0024	-0.0067	0.0184
33	0.0530	0.0269	1.1659	0.0088	0.0022	0.0023	-0.0031	0.0003	0.0000
34	-0.8421	0.0308	1.0701	-0.1501	-0.0225	-0.0201	0.0628	-0.0129	-0.0516
35	-1.2471	0.2381	1.2250	-0.6971	0.2268	0.4602	-0.4147	-0.1174	-0.0964
36	1.0832	0.1616	1.1673	0.4756	0.2959	-0.1429	0.0076	-0.1539	-0.3921
37	0.2234	0.1638	1.3486	0.0989	0.0720	-0.0256	-0.0104	-0.0617	-0.0664
38	0.6439	0.1251	1.2304	0.2435	0.1166	0.0234	-0.0072	-0.0196	-0.2159
39	-0.8666	0.1041	1.1515	-0.2954	-0.1324	0.0439	-0.0077	-0.0148	0.2449
40	-1.3854	0.0900	0.9809	-0.4357	0.1357	-0.0860	-0.0308	-0.3625	0.0409
41	-1.1502	0.0962	1.0629	-0.3753	-0.0918	-0.0960	0.2776	-0.1100	-0.1299
42	-2.2056	0.0898	0.6928	-0.6926	0.2262	-0.2123	0.0990	-0.5526	-0.1532
43	-0.4775	0.2118	1.3986	-0.2475	-0.0121	0.1093	-0.0578	-0.1055	0.1020
44	1.0495	0.1456	1.1557	0.4332	0.2867	-0.0083	-0.0606	-0.1753	-0.3437

The SAS System

The REG Procedure
Model: MODEL1
Dependent Variable: SM SM

Output Statistics

Obs	Dependent Variable	Predicted Value	Std Error Mean Predict	95% CL Mean		95% CL Predict		Residual
45	20.1000	14.8577	2.7270	9.3463	20.3692	-0.4286	30.1441	5.2423

Output Statistics

Obs	RStudent	Hat Diag H	Cov Ratio	DFFITS	DFBETAS Intercept	DFBETAS TempDiff	DFBETAS SR	DFBETAS WS	DFBETAS RH
45	0.8021	0.1494	1.2295	0.3362	-0.0159	0.0974	0.0004	0.2406	-0.1812

Sum of Residuals	0
Sum of Squared Residuals	1990.78299
Predicted Residual SS (PRESS)	2502.86261